Available online at www.sciencedirect.com
SCIENCE DIRECT®
Journal of Computational Physics 201 (2004) 80–108
JOURNAL OF COMPUTATIONAL PHYSICS
www.elsevier.com/locate/jcp

Isentropic one-fluid modelling of unsteady cavitating flow

T.G. Liu [a], B.C. Khoo [b,c,*], W.F. Xie [a]

[a] *Institute of High Performance Computing, #01-01 The Capricorn, Singapore Science Park II, Singapore 117528, Singapore*
[b] *Department of Mechanical Engineering, National University of Singapore, Kent Ridge, Singapore 119260, Singapore*
[c] *Singapore-MIT Alliance, 4 Engineering Drive 3, National University of Singapore, Singapore 117576, Singapore*

Received 4 November 2003; received in revised form 8 April 2004; accepted 5 May 2004
Available online 2 July 2004

Abstract

Unlike attached cavitation, where the cavitation boundary is steady or changes relatively slowly and periodically, the cavitation such as that observed in an underwater explosion consists of a dynamically developing boundary and can evolve to a certain dimension before collapsing very violently. The development and collapse of such cavitation is sustained mainly by the pressure jump across the cavitation boundary. In this work, the focus is on developing a one-fluid model for such cavitating flows. After the analysis and discussion are carried out for some existing one-fluid cavitation models, such as Vacuum model, Cut-off model and Schmidt's model, a mathematically more consistent one-fluid model is then developed to study the creation, evolution and collapse of such unsteady cavitation by assuming that the cavitating flow is a homogeneous mixture of isentropic gas and liquid components. In the model, both the ambient water and the mixture of cavitating flow are taken as compressible. Besides the theoretical analysis, the present model is also tested against various problems with either exact solution, or experimental data or comparison to other existing models, and then applied to a 3D underwater problem in a cylinder.

Keywords: Bulk cavitation; Homogeneous unsteady cavitating flow; Cavitation collapse; Barotropic flow; One-fluid modelling; Equation of state; Ghost fluid method

1. Introduction

Fluid-flow with cavitation occurs when the low pressure in the liquid reaches towards the limit of vapour pressure. One example is the flow generated by an underwater explosion near a structure and a free surface [19], where (bulk) cavitation just below the free surface and (hull) cavitation nearby the structure surface are usually created and collapse very violently. The dominant difficulties for simulating such kinds of cavitating flows are dynamical phase creation, dynamical interface creation, and treatment of the cavitating flow and cavitation collapse.

* Corresponding author. Tel.: +65-6874-42889; fax: +65-6779-1459.
E-mail address: mpekbc@nus.edu.sg (B.C. Khoo).

0021-9991/$ - see front matter © 2004 Elsevier Inc. All rights reserved.
doi:10.1016/j.jcp.2004.05.010

In numerical modelling of cavitating flow so far, most of the works are focused on the attached/sheet cavitation. Such cavitation normally has a fairly well-defined cavity full of vapour at saturated pressure together with a mixed wake part of bubbly flow. For the attached cavity, its shape is usually under steady/quasi-steady conditions or changes relatively slowly and/or periodically.

The numerical simulation for cavitating flow can be broadly divided into two categories: the interface tracking method and the continuum modelling method. Interface tracking method assumes that there is a clear and distinct interface between the liquid and vapour, which is determined via an iterative procedure [5,7,8]; such method is usually employed to solve the attached cavitation problem. On the other hand, a continuum method makes no attempt to track the liquid and vapour interface, but instead treats the flow as two-phases with an averaged mixture density, which continuously varies between the liquid and vapour extremes [2,6,14–16,25,30,31]. Such an approach is also sometimes called two-phase model.

The two-phase model is becoming more and more popular in recent times partly because it is able to include all the possible physics of cavitating flows. In its implementation, there are generally two different approaches. One is called the two-fluid method. The other is the one-fluid method. The first approach assumes that both phases co-exist at every point in the flow field and each phase is governed by its own set of differential equations. As a result, the total number of partial differential equations to be solved can be doubled in contrast to the single-phase flow [24]. This approach is also extensively applied to simulate compressible multi-medium flows [3,9,29]. Because the exchange of mass, momentum and energy is treated explicitly as transfer terms in this approach, the two-fluid model can relatively easily take into account the physical details occurring at the cavitating interface such as mass/energy exchange, thermal transfer and even surface tension. However, some quantities such as exchange rates [2,16,25,30] and the viscous friction between the two phases [15,25] have to be known a priori; such quantities are usually very difficult to be obtained whether experimentally or otherwise. On the contrary, the one-fluid method treats the cavitating flow as a mixture of two fluids behaving as one. Thus, one set of differential equations similar to the single-phase flow expresses the whole fluid motion. The most difficult part for this approach is to define a proper constitutive relation (equation of state) for the mixture to close the system [6,26,31]. In order to define the constitutive relation, the mixture is usually supposed or assumed to be homogeneous and barotropic [6,26]. If possible, one can also define this relation using the tabulated mixture properties similar to that carried out in [31] for simulating water and vapour mixture. Because the flow parameters obtained are in the averaged sense for the one-fluid model, it is difficult for such a model to resolve the detailed physics or quantities related to detailed phase transition. However, it is very easy to treat the dynamic creation and collapse of cavitation (as will be shown in Section 3).

Instead of the abovementioned steady attached/sheet cavitation, the present interest is on unsteady cavitation, which consists of a dynamically developing boundary and commonly observed in the underwater explosion, where both the ambient liquid and the mixture have to be considered as compressible; the development and collapse of such cavitation is sustained mainly by the pressure jump across the cavitation boundary. In contrast to the attached/sheet cavitation, where relatively extensive studies have been carried out, there is much less work on the latter in literature. Because the cavitation dimension and pressure surge caused by cavitation collapse are the major concerns in the underwater explosion, the developed methods for modelling such cavitating flows are usually one-fluid methods and governed by the Euler equations, where the flow viscosity, thermal conductivity, surface tension and turbulence are generally neglected. The commonly used one-fluid models for such cavitating flow are the Cut-off model and the Vacuum model. Both are essentially pure-fluid models and no phase exchange is taken into account. In the Cut-off model like those used by Aanhold et al. [1] and Wardlaw and Luton [33], flow pressure is simply re-instated as a given value and computation continues whenever the liquid pressure is detected lower than a given critical level. In the pressure cut-off (cavitating) region, the flow medium is still the same liquid and no phase change is considered. The Cut-off model is quite easy to implement and use. However, there are obvious physical violations; the conservation law may not be maintained and the hyperbolic system of equations is

non-physically degenerated due to the pressure and the associated density cut-off and the zero sound speed in the cavitating region. The Vacuum model treats the cavitation zone of zero mass inside and is an ideal approximation of the cavitation. This model is physically reasonable because usually only a small amount of liquid transforms into vapour and the vapour density is about $O(10^{-4})$ of the liquid density. The idea of neglecting the amount of vapour is also used in the simulation of attached/sheet cavitation [15]. Tang and Huang [27] developed a vacuum model to study 1D inviscid cavitating flow. Their vacuum model was based on the solution of a local gas–liquid–vacuum Riemann problem. Although it is well established both mathematically and numerically for 1D inviscid compressible cavitating flow, the extension of this model to multi-dimensions, as we are aware, has yet to be established probably due to the (difficult) requirement of constructing a local Riemann solver, where the vacuum boundary needs to be traced and a special Riemann problem in the neighbourhood of the vacuum region has to be solved. Schmidt et al. [26] developed a one-fluid model for modelling high-speed cavitating nozzles. Schmidt's model is applicable for small size cavitation of high pressure. To extend the application of this model to the water hammer phenomenon, Qin et al. [21] incorporated a model constant into Schmidt's model. However, by a strict mathematical analysis, this model constant, which was chosen to be in the range from 10^{-3} to 10^{-5}, should be determinable and equal to one if one requires that the equation of state developed for the cavitating flow is mathematically consistent with the formulation of sound speed used.

The two-fluid model is seldom employed to the present flow of interest on unsteady cavitation because the parameters relating to phase exchange are generally unknown. The multi-phase (two-fluid) model developed by Saurel and co-workers [11,23,24] has been shown applicable to a range of problems involving multi-phase and multi-medium compressible flows. This is, however, a quite complicated model involving non-conservative terms related to phase exchange. To simulate cavitating flow using this model, the initial pure liquid has to be supposedly mixed with a negligible amount of vapour. Thus far, we are only aware that this model has been used to simulate cavitating flow of Case 2 as detailed in Section 4.

Because the present interest lies in the simulation of unsteady cavitation as (possibly) occurring in an underwater explosion, the influence of flow viscosity, turbulence, thermal non-equilibrium and cavitation surface tension are considered as secondary and neglected. Since the cavitation dimension and cavitation collapse (pressure surge) are the primary concerns and coupled with difficulty to determine the physical phase exchange rates for such cavitating flows, we have decided to suppress the explicit phase transfer terms in the present work by using the *one-fluid model*. This leads naturally to one main objective in this study to develop a pertinent equation of state for the mixture. Due to the employment of Tait's EOS, which is homogeneous and isentropic, the present one-fluid model for the mixture is therefore developed under the same assumptions of homogeneous and isentropic gas and liquid components.

One may have observed that, to reflect the compressibility characteristics of cavitating flow, some two-phase models developed for simulating the attached/sheet cavitation simply employ the standard sound-speed formula of homogeneous mixture in [4,32] to define the sonic speed but still assume the liquid component to be incompressible in the mixture region. It should be noted that this homogeneous sound-speed formula should be strictly obtained by assuming both the liquid and vapour components are compressible. Thus, there is an apparent mathematical inconsistency inherent in such two-phase models. Although satisfactory results may be provided when applied to the attached/sheet cavitation, inaccuracies or incorrect solution can occur when applied to larger size or unsteady cavitation problems. To better understand the existing one-fluid models, a careful analysis on each will also be carried out in this work. To remove the mathematical inconsistence as mentioned above, the key is to accurately find the relationship between pressure and void fraction; for homogeneous and isentropic flow, we argue that the change of void fraction cannot be independent of pressure and should be a function of pressure alone. Overall, we expect the present proposed one-fluid cavitation model to exhibit several key features:

- Relatively easy to use.
- No new governing equation to be added.

- All phases including the mixture taken as compressible.
- The dynamic creation, evolution and collapse of cavitation.
- No mathematical and physical inconsistency under the assumptions used.

One will also find that the present model is very easy to extend to multi-dimensions. This work will focus on the development and analysis of the present cavitation model, which will be validated by either comparison to the analytical solution, or experimental results or existing models, and then applied to a 3D underwater explosion in a closed cylinder. Important conclusions will also be obtained vis-à-vis the analysis carried out for the existing Vacuum model, Cut-off model and Schmidt's model.

The text below is arranged as follows. In Section 2, the 1D Euler equations for compressible water, vapour and mixture are presented. The jump relationship across the cavitation boundary is also discussed. Moreover, some (important) conclusions will be reached on the behaviours of cavitation in the inviscid one-fluid model. In Section 3, an isentropic one-fluid cavitation model will be developed and the relationship between the void fraction and pressure will also be obtained. There is discussion and analysis carried out for the Cut-off model and Schmidt's model. Furthermore, some conclusions will also be reached about these existing models. In Section 4, several problems are employed to test and verify the present cavitation model. In this section, the present model developed is then applied to a 3D underwater explosion in a closed cylinder, where shock–cavitation interaction and cavitation collapse occur. A brief summary is given in Section 5.

2. Governing equation

In the present study, the cavitation to be considered in an underwater explosion has a dynamically developing boundary. There is no information whether experimentally or otherwise on the local transfer rates between liquid and vapour. Thus, we chose to utilise the one-fluid model to suppress these transfer terms by assuming that the mixture of liquid and vapour is homogeneous, barotropic and no heat conductivity. These are the usual and realistic assumptions for simulating cavitation occurring in cold water and under high pressure condition in as an underwater explosion in the employment of the inviscid Euler equation system. Since the governing equations used in the present study are the inviscid Euler equations for compressible flows, effects of flow viscosity, turbulence, surface tension of interfaces and thermal non-equilibrium are neglected.

2.1. Euler equation for barotropic flow

The 1D conservative equations for inviscid barotropic gas, water or bubbly flow can be written in a consistent form as

$$\frac{\partial U}{\partial t}+\frac{\partial F(U)}{\partial x}=0, \tag{2.1}$$

$$p=p(\rho), \tag{2.2}$$

$$\rho=\alpha\rho_{\mathrm{g}}+(1-\alpha)\rho_{\ell}. \tag{2.3}$$

Here $U=[\rho,\rho u]^{\mathrm{T}}$, $F(U)=[\rho u,\rho u^2+p]^{\mathrm{T}}$, ρ is the (averaged) flow density, u is the (averaged) flow velocity, p is the (averaged) flow pressure, ρ_{ℓ} is the pure liquid density, ρ_{g} is the pure gas (vapour) density and α is the void fraction. If α is set to 0, it becomes a pure liquid flow, while if α is set to 1, the flow is a pure gas

(vapour). Note that the system of equations (2.1) and (2.2) is closed for the pure liquid or gas medium. It is not so for the mixture unless a way of determining α is given or provided.

In the mixture, the vapour component is assumed homogeneous, isentropic and compressible. Then we have

$$\frac{p}{p_0} = \left(\frac{\rho_g}{\rho_{g0}}\right)^{\gamma}. \tag{2.4}$$

Here γ is the ratio of specific heats and set to 1.4 in the present study unless otherwise specified, and ρ_{g0} is the gas density at pressure p_0 The water (liquid) medium and the liquid component in the mixture are also assumed compressible and isentropic. In particular, we employ Tait's equation, thereby giving rise to the relation between pressure and water density as

$$p = B\left(\frac{\rho_\ell}{\rho_{\ell 0}}\right)^N - B + A \quad \text{or} \quad \frac{\bar{p}}{\bar{p}_0} = \left(\frac{\rho_\ell}{\rho_{\ell 0}}\right)^N. \tag{2.5}$$

Here B and A are constants and set equal to 3.31×10^8 and 10^5 Pa, respectively, $p_0 = A$ and $\rho_{\ell 0} = 1000$ kg/m^3 are initial pressure and density for water, $\bar{p} = p + \bar{B}$, $\bar{p}_0 = p_0 + \bar{B}$, $\bar{B} = B - A$, and N is a constant set to 7.15. The sound speeds associated with (2.4) and (2.5) can be expressed, respectively, by

$$a_g = \left(\frac{\mathrm{d}p}{\mathrm{d}\rho_g}\right)^{1/2} = \left(\gamma\frac{p}{\rho_g}\right)^{1/2} \tag{2.6}$$

and

$$a_\ell = \left(\frac{\mathrm{d}p}{\mathrm{d}\rho_\ell}\right)^{1/2} = \left(N\frac{\bar{p}}{\rho_\ell}\right)^{1/2}. \tag{2.7}$$

Tait's equation is the simplest form of EOS for compressible water flow. It works well when the pressure is below 20,000 atm [12].

The EOS for the mixture will be developed in Section 3, which is a major goal of the present work.

2.2. Relationship across the cavitation boundary

As mentioned above, the evolution of an unsteady cavitation may entail a pressure jump across the cavitation boundary. As so, this gives rise to a local jump relation, which governs the motion of the cavitation boundary. Assuming that there is a cavitation interface (boundary), x_I in the cell $[x_A, x_B]$, and the liquid is located in $[x_A, x_I]$, while the mixture occupies $[x_I, x_B]$, using the integral–differential form of (2.1), we have

$$\frac{\mathrm{d}}{\mathrm{d}t}\int_{x_A}^{x_B} U\,\mathrm{d}x + F_B - F_A = 0, \tag{2.8}$$

where $F_B = F(U(x_B, t))$ and $F_A = F(U(x_A, t))$. On the other hand, by using the following differential–integral equality

$$\frac{\mathrm{d}}{\mathrm{d}t}\int_{a(t)}^{b(t)} U(x,t)\,\mathrm{d}x = \frac{\mathrm{d}b}{\mathrm{d}t}U_b - \frac{\mathrm{d}a}{\mathrm{d}t}U_a + \int_{a(t)}^{b(t)} \frac{\partial U}{\partial t}\,\mathrm{d}x, \tag{2.9}$$

over the variable intervals $[x_A, x_I]$ and $[x_I, x_B]$, and substituting (2.1) into the right-hand side integral term of (2.9), we obtain

$$\frac{\mathrm{d}}{\mathrm{d}t}\int_{x_A}^{x_I} U(x,t)\,\mathrm{d}x = \frac{\mathrm{d}x_I}{\mathrm{d}t}U_\ell^{\mathrm{I}} + F_A - F_\ell^{\mathrm{I}} \tag{2.10}$$

and

$$\frac{\mathrm{d}}{\mathrm{d}t}\int_{x_I}^{x_B} U(x,t)\,\mathrm{d}x = -\frac{\mathrm{d}x_I}{\mathrm{d}t}U_{\mathrm{m}}^{\mathrm{I}} + F_{\mathrm{m}}^{\mathrm{I}} - F_B, \tag{2.11}$$

respectively. Summing (2.10) and (2.11), and using (2.8), we obtain the jump relationship across the moving cavitation interface as

$$s(U_\ell^{\mathrm{I}} - U_{\mathrm{m}}^{\mathrm{I}}) = F_\ell^{\mathrm{I}} - F_{\mathrm{m}}^{\mathrm{I}}. \tag{2.12}$$

Here $U_\ell^{\mathrm{I}} = \lim_{x\to x_I-} U(x,t)$ and $U_{\mathrm{m}}^{\mathrm{I}} = \lim_{x\to x_I+} U(x,t)$, $F_\ell^{\mathrm{I}} = F(U_\ell^{\mathrm{I}})$, $F_{\mathrm{m}}^{\mathrm{I}} = F(U_{\mathrm{m}}^{\mathrm{I}})$ and $s = \mathrm{d}x_I/\mathrm{d}t$. Hereafter, the subscripts "ℓ" and "m" indicate the "liquid" and "mixture" media, respectively. The superscript "I" stands for "Interface" (cavitation boundary). (2.12) leads to the Rankine–Hugoniot relationship for the propagation of an unsteady cavitation boundary in association with the inviscid one-fluid modelling (2.1). (2.12) can be rewritten as

$$\rho_\ell^{\mathrm{I}} v_\ell^{\mathrm{I}} = \rho_{\mathrm{m}}^{\mathrm{I}} v_{\mathrm{m}}^{\mathrm{I}}, \tag{2.13a}$$

$$\rho_\ell^{\mathrm{I}} (v_\ell^{\mathrm{I}})^2 + p_\ell^{\mathrm{I}} = \rho_{\mathrm{m}}^{\mathrm{I}} (v_{\mathrm{m}}^{\mathrm{I}})^2 + p_{\mathrm{m}}^{\mathrm{I}}, \tag{2.13b}$$

where $v_\ell^{\mathrm{I}} = u_\ell^{\mathrm{I}} - s$ and $v_{\mathrm{m}}^{\mathrm{I}} = u_{\mathrm{m}}^{\mathrm{I}} - s$. Some important conclusions can be deduced from (2.12) or (2.13).

Corollary 2.1. *The inviscid one-fluid model allows the existence of a steady cavitation or cavitation convecting with the local flow velocity.*

For steady cavitation or cavitation convecting with the local fluid velocity, the averaged pressure and averaged normal velocity are continuous across the cavitation interface. In such a situation, (2.13) degenerates to a relationship of "contact discontinuity". As a result, the unsteady one-fluid model includes the possibility of attached/sheet cavitation. The density jump indicates the possible sudden jump of void fraction across the cavitation boundary.

Corollary 2.2. *A shock front cannot be connected to a vacuum* [28]; *the cavitation interface moves with the local liquid velocity and the pressure varies continuously across the interface using the Vacuum model.*

Since the mass $\rho_{\mathrm{m}}^{\mathrm{I}}$ is zero inside the vacuum, (2.13a) implies that $u_\ell^{\mathrm{I}} = s$, which then results in $p_\ell^{\mathrm{I}} = p_{\mathrm{m}}^{\mathrm{I}}$ by (2.13b). This completes the proof for Corollary 2.2. Since a vacuum does not allow to be connected to a shock front or singularity, the (pressure or velocity) singularity created at the vacuum boundary during the vacuum collapse or the shock–vacuum interaction has to be simultaneously decomposed. This requires the constructing of a proper type of Riemann solution. The details of constructing such a type of Riemann solution can be found in [27].

Corollary 2.3. *With the exception of the Vacuum model, a pure liquid model of cavitation leads to the propagation of cavitation boundary with a "shock speed" if there is a pressure jump across the cavitation interface. Furthermore, relative to the cavitation interface, the local flow velocity is supersonic inside the cavitation, while it is subsonic in the liquid during cavitation collapse.*

In Corollary 2.3, we have assumed that Tait's equation is employed for the liquid and the pressure (density) inside the cavitation is lower than the neighbouring medium. Because the liquid flow is assumed as for pure phase even in the cavitation region, (2.12) recovers to the "shock" relationship for the pure phase flow. Thus the cavitation interface propagates like a "shock" front if there is a pressure jump across the propagating front. During the expansion of the cavitation region, the flow pressure and density decrease across the cavitation front and the cavitation boundary moves with an "expansion shock" speed. The appearance of such "expansion shock" is due to the degeneration of EOS from a convex to non-convex type, as will be discussed and shown in Section 3. On the contrary, during the collapse of cavitation, the flow pressure and density increase across the cavitation interface, the cavitation boundary acts as a genuine shock front. This concludes the proof for the first part of Corollary 2.3. The proof of the second part can be found in [18]. Corollary 2.1 has stated that the cavitation boundary can propagate as a contact discontinuity even in the pure-phase model. The interface tracking method such as those developed by Chen and Heister [5] and Deshpande et al. [7,8] for the attached cavitation essentially functions like a Cut-off model, where the fluid inside the cavity can be assumed as liquid of saturated pressure without significant effect on the final results.

Corollary 2.4. *If the sonic speed and density in the cavitation region are lower than those in the liquid at the vapour (saturated) pressure, then we have* $M_\ell^{\mathrm{I}} < M_{\mathrm{m}}^{\mathrm{I}}$.

Here, M ($M = |u - s|/a$) is the Mach number relative to the propagating cavitation interface. Expression (2.13a) can be rewritten as $M_\ell^{\mathrm{I}} = M_{\mathrm{m}}^{\mathrm{I}}(\rho_{\mathrm{m}}^{\mathrm{I}} a_{\mathrm{m}}^{\mathrm{I}}/\rho_\ell^{\mathrm{I}} a_\ell^{\mathrm{I}})$. Thus Corollary 2.4 is fairly obvious from the given conditions. This Corollary implies that the flow relative to the cavitation motion may be transonic or even supersonic in the cavitation region. This is true especially during the collapse of cavitation.

Corollary 2.5. *If the vapour pressure is set low enough but still positive and* $M_\ell^{\mathrm{I}} < \sqrt{B/\bar{p}_\ell^{\mathrm{I}}}$, *then there does not exist one liquid flow status* $(\rho_\ell^c, p_\ell^c, u_\ell^c)$ *of* $\rho_\ell^{\mathrm{sat}} \leqslant \rho_\ell^c < \rho_\ell^{\mathrm{I}}$ and $p_\ell^{\mathrm{sat}} \leqslant p_\ell^c < p_\ell^{\mathrm{I}}$ *such that* (a) $\rho_\ell^{\mathrm{I}} v_\ell^{\mathrm{I}} = \rho_\ell^c v_\ell^c$ *and* (b) $\rho_\ell^{\mathrm{I}}(v_\ell^{\mathrm{I}})^2 + p_\ell^{\mathrm{I}} = \rho_\ell^c (v_\ell^c)^2 + p_\ell^c$.

One can refer to Appendix A for the proof of this corollary. Here $v_\ell^c = u_\ell^c - s$, s satisfies (2.12) or (2.13), and the pressure and density follows Tait's EOS. ρ_ℓ^{sat} is the corresponding liquid density at the given vapour (saturated) pressure, p_ℓ^{sat}. In general, the EOS for the mixture is different from that of the surrounding liquid. Thus, numerical oscillations may occur in the vicinity of cavitation interface if the numerical schemes developed for single-phase flows are directly employed to simulate the cavitating flow. One of the effective techniques developed to suppress such non-physical oscillations is the Ghost Fluid Method [10,20], where the solution of flow is obtained essentially by carrying out computation in the single medium via defining the ghost fluid status. This corollary suggests that it may not be possible to define the ghost fluid status to maintain the Rankine–Hugoniot condition if there is a pressure jump across the cavitation interface. This implies that such method applied to unsteady cavitating flow may not work as efficiently or well as compared to application to multi-medium flows. It does not, however, exclude this novel technique in its application to simulate steady or quasi-steady cavitation/cavity.

Remark 1. It is fairly obvious that (2.12) holds for multi-dimensional inviscid one-fluid modelling; all the conclusions obtained above are valid in the normal direction in multi-dimensions.

3. Unsteady cavitation models

Before we develop the present unsteady one-fluid cavitation model, we shall briefly introduce the Cut-off model and Schmidt's model since these will be employed for further analysis and comparison to the present model.

3.1. The Cut-off model

The Cut-off model sets the pressure equal to a given value (saturated vapour pressure) when the flow pressure falls down below a critical pressure level. If Tait's equation is employed for the pure water, the EOS for this model can then be described as

$$p = \begin{cases} B\left(\frac{\rho}{\rho_0}\right)^N - B + A, & \rho > \rho_{\text{sat}}, \\ p_{\text{sat}}, & \rho \leqslant \rho_{\text{sat}}. \end{cases} \tag{3.1}$$

Here, ρ_{sat} is the liquid density in association with the given critical pressure p_{sat}. We have the following conclusion for the Cut-off model.

Conclusion 3.1. Using the Cut-off model (3.1), the EOS degenerates from a convex type in the pure liquid region to a non-convex form in the pressure cut-off region. Furthermore, the sound speed becomes zero and thus the system (2.1) is affected and degenerated in the pressure cut-off (cavitation) region.

At the location of cavitation initialisation and creation, the density is usually set to ρ_{sat}. As a result, mass loss occurs and which results in the violation of conservation law. However, this violation may be avoided for the barotropic flow if the updated density is maintained without cut-off. To maintain the conservative computation using the Cut-off model, the system has to be artificially kept hyperbolically and thus a positive sound speed, which cannot be consistent with (3.1), has to be defined in the cavitation region. The sound speed can be defined by either assuming a constant value at the given critical pressure or employing expression (2.7), where the pressure is the fixed critical pressure and the density is updated from the conservative computation. Doing so, there are several adverse consequences. Firstly, the numerical sound speed in the cavitation region can be equal to or larger than that of the surrounding medium, which is not physically true, and the calculation of sound speed contradicts the assumed EOS (3.1). Secondly, the flow status computed inside the cavitation region is not physical. Thirdly, the motion of cavitation boundary is forced to propagate with a "shock" speed (Corollary 2.3). Fourthly, the inconsistency of above *artificial* treatment on the sound speed with EOS (3.1) tends to exclude an "expansion shock", resulting in the decomposition of this "expansion shock" under such treatment. Lastly, the result of captured cavitation collapse may not be physical and possibly inaccurate. The first and second consequences are obvious. Due to the pressure cut-off, a pressure jump is actually created across the cavitation boundary (this is also the physical requirement for sustaining the development of the unsteady cavitation). Since the Cut-off model is a pure phase model, the conservative computation using this model forces the satisfaction of Rankine–Hugoniot relationship at the cavitation boundary. This leads to the motion of cavitation boundary following the shock relationship as shown in Corollary 2.3. The expansion of cavitation with an "expansion shock" speed is mathematically allowed due to the EOS degeneration. This is consistent with the physical observation that across the expanding cavitation front, the pressure drops to or below the vapour pressure. On the other hand, the above treatment for the zero sonic speed forces the non-convex type EOS (3.1) in the cavitation region to function like a convex type, where an expansion shock is not allowed physically. Thus, both mathematical and physical conflicts occur across the cavitation boundary under such treatment. Numerical results will show in Section 4 that two or more steps of small pressure jump across the cavitation

boundary occur (i.e. the initial one step pressure jump is decomposed into two or more steps of smaller pressure jump). However, numerical tests in Section 4 will also show that the inaccuracy caused by the non-physical and inconsistent treatment of the cavitation region does not affect too severely for the calculated peak pressures. This may be the reason this model is still popularly employed in the simulation of underwater explosions and also implemented in some commercial software. On the other hand, the results of cavitation collapse as captured by this model are observed to be not so accurate.

3.2. Schmidt's model

This is another (unsteady) one-fluid compressible cavitation model in literature, which was developed and verified for high velocity and high pressure flow in a very small nozzle. In this model, the cavitating flow is assumed to be a homogeneous and barotropic mixture of gas and liquid, where the sound speed can theoretically be given [4,32] as

$$a = \left\{ \left[\alpha.\rho_{\mathrm{g}} + (1-\alpha).\rho_{\ell}\right].\left[\frac{\alpha}{\rho_{\mathrm{g}}.a_{\mathrm{g}}^2} + \frac{(1-\alpha)}{\rho_{\ell}.a_{\ell}^2}\right] \right\}^{-1/2}. \tag{3.2}$$

To obtain the barotropic EOS for the mixture, Schmidt et al. [26] assumed the sound speeds for the gas and liquid components as well as their respective densities to be constant, and the mixture follows the constitutive relation of $\mathrm{d}p/\mathrm{d}\rho = a^2$. As a result, the pressure can be obtained analytically as a function of void fraction by integrating $\mathrm{d}p/\mathrm{d}\rho = a^2$ using (3.2), giving rise to the EOS,

$$p = p'_{\mathrm{sat}} + p_{gl}.\ln\left[\frac{\rho_{\mathrm{g}}.a_{\mathrm{g}}^2.(\rho_{\ell} + \alpha.(\rho_{\mathrm{g}} - \rho_{\ell}))}{\rho_{\ell}.\left(\rho_{\mathrm{g}}.a_{\mathrm{g}}^2 - \alpha\left(\rho_{\mathrm{g}}.a_{\mathrm{g}}^2 - \rho_{\ell}.a_{\ell}^2\right)\right)}\right], \tag{3.3}$$

where p_{gl} is a parameter of the known surrounding fluid properties given as

$$p_{gl} = \frac{\rho_{\mathrm{g}}.a_{\mathrm{g}}^2.\rho_{\ell}.a_{\ell}^2.(\rho_{\mathrm{g}} - \rho_{\ell})}{\rho_{\mathrm{g}}^2.a_{\mathrm{g}}^2 - \rho_{\ell}^2.a_{\ell}^2}. \tag{3.4}$$

Once the mixture density is obtained, the void fraction can be calculated from (2.3) on the assumption of constant densities of vapour and liquid components. This is a physically stable model. However, the "saturated" pressure p'_{sat} has to be carefully obtained. It can be shown mathematically that if p'_{sat} is not large enough the "pressure" obtained from (3.3) may be negative when the void fraction, α, takes on a value larger than $\alpha_{\min}$, which is given by

$$\alpha_{\min} = \frac{\rho_{\ell}\rho_{\mathrm{g}}a_{\mathrm{g}}^2(1 - e^{-p'_{\mathrm{sat}}/p_{gl}})}{(\rho_{\ell} - \rho_{\mathrm{g}})\rho_{\mathrm{g}}a_{\mathrm{g}}^2 + \rho_{\ell}(\rho_{\ell}a_{\ell}^2 - \rho_{\mathrm{g}}a_{\mathrm{g}}^2)e^{-p'_{\mathrm{sat}}/p_{gl}}}. \tag{3.5}$$

Physically, the negative pressure should not be allowed to occur. By assuming $\alpha_{\min}$ is equal to 1, the minimum, $p'_{\min}$ (of p'_{sat} mathematically required for ensuring positive pressure for α taken from 0 to 1), is

$$p'_{\mathrm{sat}} \geqslant p'_{\min} = -p_{gl}.\ln\left[\frac{\rho_{\mathrm{g}}^2.a_{\mathrm{g}}^2.}{\rho_{\ell}^2 a_{\ell}^2.}\right]. \tag{3.6a}$$

$p'_{\min}$ can also be obtained by setting $p = 0$ at $\alpha = 1$ in (3.3) or integrating equation (2.2) from pressure of zero and density of nearly zero at $\alpha = 1$ to the "saturated" density at $\alpha = 0$ [26]. One can easily check that

the "saturated" pressure p'_{sat} in the vapour phase of the cavitation region given in (3.3) is overestimated. To better understand the possible limitation of Schmidt's model, we can express p'_{min} approximately as follows:

$$p'_{min} \approx -2\rho_{g\cdot}a^2_{g\cdot}\left(\ln\frac{\rho_{g\cdot}}{\rho_{\ell\cdot}} + \ln\frac{a_{g\cdot}}{a_{\ell\cdot}}\right). \tag{3.6b}$$

Here $\ln(a_g/a_\ell)$ usually ranges from -1 to -3. If the ratio, ρ_g/ρ_ℓ, is set to $1.0E-5$ as applied in [26], p'_{min} is a value of about 20 kPa. With the decrease of ρ_g/ρ_ℓ, one can easily check that p'_{min} can decrease to the physically reasonable saturated pressure ranging from several thousands to hundreds of Pascal. On the other hand, the larger ρ_g/ρ_ℓ can lead p'_{min} to the unphysical range. For examples, the magnitude of p'_{min} approaches 1 bar when ρ_g/ρ_ℓ increases to $1.0E-4$; it can even assume a quantity beyond 10 bar when ρ_g/ρ_ℓ approaches $1.0E-3$. The above analysis suggests that Schmidt's model may only work properly with ρ_g/ρ_ℓ about or below $1.0E-5$. With the expansion of cavitation dimension, the pressure jump across the cavitation interface decreases or even disappears. Or if the initial surrounding pressure is not very high, the ratio of ρ_g/ρ_ℓ can be in the range of $1.0E-4$ to $1.0E-3$, thereby resulting in the inapplicability of Schmidt's model. The requirement of quite low density ratio of ρ_g/ρ_ℓ for Schmidt's model indicates a possible large pressure jump across the cavitation interface. This can occur in the flow situation of high surrounding pressure and where the cavitation size is small. This is possibly one reason why this model can work effectively for the high pressure flow in the small size nozzle [26].

When applying this model to the large size cavitation or low pressure situations, one has to set the ratio of ρ_g/ρ_ℓ to be about or below $1.0E-5$. In the present test and study of using Schmidt's model, the liquid flow is always assumed to cavitate under the physical p_{sat}. We have found that the (required) large value of p'_{sat} indeed limits the wide applications of this model. This is because such a fixed large p'_{sat} can lead to a non-physical cavitation pressure in the neighbourhood of the cavitation interface, which is unreasonably higher than the surrounding flow pressure; this can happen when the cavitation region evolves to take on larger dimension. With the cavitation development, the surrounding liquid pressure calculated next to the cavitation interface may decrease rapidly to a magnitude that can be far smaller than p'_{sat} and even close to the physical p_{sat}, which is the limit of the EOS valid for the surrounding flow, while the flow pressure inside the cavitation in the vicinity of cavitation interface may bear a magnitude of about p'_{sat}. Physically, this model should not be applied beyond the limit of the surrounding pressure magnitude decreasing to lower than p'_{sat} as analysed above. Otherwise, the non-physical higher pressure inside the cavitation than the surrounding inevitably causes numerical oscillations in the computation. As a result, the efficiency of using this model is low because a small CFL number has to be used to suppress the oscillations. On the other hand, if the pressure jump across the cavitation interface is large enough such that the surrounding pressure always maintains higher than that inside the cavitation, numerical oscillations do not occur in the computation. Such situations could occur in the simulation of high pressure flow involving small-size cavitation.

Qin et al. [21] presented a modification of Schmidt's model by multiplying a parameter (β) of $O(10^{-3})$ to $O(10^{-5})$ to the second term of (3.3) accordingly. In doing so, the "saturated" pressure p'_{sat} can be adjusted to the physical p_{sat}. Such a modification also essentially makes the model takes on the characteristic of a pressure cut-off. This is because the product of β and the second non-constant term in (3.3) is negligibly small. On the other hand, such a modification makes the resultant EOS apparently inconsistent with (3.2).

There are mathematical inconsistencies between (3.2) and (3.3). In fact, one of the limitations of Schmidt's model arises from these inconsistencies. In the derivation of (3.2), both the gas and liquid components are assumed compressible; the sound speeds and densities of both components are functions of pressure. Thus, the assumption of constant component densities and sonic speeds utilised in obtaining (3.3) contradicts the premises of (3.2). Besides Schmidt's EOS (3.3), there are some other barotropic relations developed and discussed in [4] by either assuming the density and sonic speed of the liquid component are constant or neglecting the density of the gas component or the volume of liquid component. Those

barotropic relations did provide satisfactory results in the respective applicable ranges. However, the mathematical inconsistencies between the barotropic relations and the sound speed (3.2) invariably exist. We argue that these inconsistencies are removable for barotropic mixture. This is the motivation and task of the present work to develop a mathematically sound barotropic EOS based on (3.2).

Because the sound speed formulation used for Schmidt's model is mathematically sound and verified experimentally, it is the inconsistent way of deriving EOS (3.3) that leads to a very large p'_{sat} obtained, which results in inherent limitation when applied to large-size cavitation. This shortcoming causes very stringent CFL used especially for the low-pressure surrounding flow or large size cavitation, as will be shown in Section 4.

3.3. The present unsteady one-fluid model

The sound speed provided by (3.2) is mathematically sound and accurate in the comparison to experimental results as shown in [4,32] for the homogeneous and thermal equilibrium mixture with the neglect of the influence of mass transfer on the sound speed. This formulation was also recently employed by Ahuja et al. [2] and Venkateswaran et al. [30] in the simulation of attached cavitation with consideration of the compressibility effect in the mixed region. There is no fundamental reason to discard or dismiss (3.2) applicable to the flow, which is assumed homogeneous and in thermal equilibrium. Once the mixture is assumed homogeneous and in thermal equilibrium, the barotropic relation for the mixture should be determinable without any contradiction with respect to (3.2). In fact, if the mixture and the gas and liquid components are assumed barotropic, the void fraction can only be a function of pressure alone due to (2.3). Therefore, we have the following conclusions.

Conclusion 3.2. For barotropic, homogeneous and thermal equilibrium mixture of gas and liquid, by neglecting the influence of mass transfer on the sound speed, the local sound speed of the mixture follows (3.2), and the void fraction is governed by

$$\frac{\mathrm{d}\alpha}{\mathrm{d}p}(\rho_\ell - \rho_{\mathrm{g}}) = \alpha\frac{\mathrm{d}\rho_{\mathrm{g}}}{\mathrm{d}p} + (1-\alpha)\frac{\mathrm{d}\rho_\ell}{\mathrm{d}p} - \frac{\mathrm{d}\rho}{\mathrm{d}p}. \tag{3.7}$$

The detailed derivation leading to (3.2) can be found in [4,31]. One can easily obtain (3.7) by taking the derivative of (2.3) with respect to pressure. Here the compressibility of the mixture comes from the gas and liquid components as well as void fraction. Since (2.3) is always held, (3.7) is true and should be maintained consistently with (3.2). By assuming both the gas and liquid components and the mixture follow the constitutive relation of $\mathrm{d}p/\mathrm{d}\rho = a^2$ and using (3.2), expression (3.7) can then be reduced to the form

$$\frac{\mathrm{d}\alpha}{\mathrm{d}p} = \alpha(1-\alpha)\left(\frac{1}{\rho_\ell a_\ell^2} - \frac{1}{\rho_{\mathrm{g}} a_{\mathrm{g}}^2}\right). \tag{3.8}$$

We are able to develop a sound barotropic EOS for the mixture if the vapour and liquid components are assumed isentropic. In fact, we have further conclusions based on (3.2) and (3.8).

Conclusion 3.3. If the gas and liquid components are assumed isentropic, by integrating (3.8) and (3.2), we have

$$\frac{\alpha}{1-\alpha} = k\frac{(\bar{p}/\bar{p}_{\text{cav}})^{1/N}}{(p/p_{\text{cav}})^{1/\gamma}} \tag{3.9}$$

and

$$\rho = \frac{k\rho_{\mathrm{g}}^{\mathrm{cav}} + \rho_{\ell}^{\mathrm{cav}}}{\left(\frac{\bar{p}}{\bar{p}_{\mathrm{cav}}}\right)^{-1/N} + k\left(\frac{p}{p_{\mathrm{cav}}}\right)^{-1/\gamma}}, \tag{3.10}$$

where $k = \alpha_0/(1-\alpha_0)$. $\rho_{\mathrm{g}}^{\mathrm{cav}}$ and $\rho_{\ell}^{\mathrm{cav}}$ are the associated gas and liquid density at the cavitation pressure p_{cav}, respectively, α_0 is the known void fraction of the mixture density at p_{cav}. The validity of (3.9) is given as follows. Using (2.6) and (2.7), (3.8) can be rewritten as

$$\frac{\mathrm{d}\alpha}{\mathrm{d}p} = \alpha(1-\alpha)\left(\frac{1}{N\bar{p}} - \frac{1}{\gamma p}\right) \tag{3.11}$$

or

$$\mathrm{d}(\ln\alpha) - \mathrm{d}(\ln(1-\alpha)) = \mathrm{d}(\ln\bar{p}^{1/N}) - \mathrm{d}(\ln p^{1/\gamma}). \tag{3.12}$$

From (3.12), it can be deduced that α is not allowed to be equal to 0 or 1. Physically a void fraction jump exists across the cavitation interface. Assuming that the pressure drops to p_{cav} ($p_{\mathrm{cav}} \leqslant p_{\mathrm{sat}}$) and the void fraction takes on the value of α_0 simultaneously across the cavitation interface, (3.9) is obtained by integrating (3.12) from p_{cav}. Substituting of α from (3.9) into (2.3), EOS (3.10) is obtained and which is consistent with (3.2) regardless of k or α_0. This completes the proof of Conclusion 3.3. From Conclusion 3.3 and (3.12), it can be further deduced the following important consequences.

Corollary 3.1. *For the present one-fluid model in the mixture region, we have*:

(I) *p is a one-to-one monotonous function of ρ and there is a unique positive p for each $\rho > 0$.*
(II) *The mixture density approaches zero as the pressure goes to zero.*
(III) *The void faction approaches 1 when the pressure goes to zero.*
(IV) *The sound speed approaches zero when the pressure goes to zero.*
(V) *A void fraction jump must occur across the cavitation boundary.*
(VI) *The whole system (2.1) is hyperbolic and conservative.*

The jump of the void fraction across the cavitation interface is not explicitly excluded by (3.9) and (3.10) but it is made implicitly by (3.12). As the void fraction jump is usually very small during the development of cavitation, it can be easily smeared out by the numerical viscosity of the scheme.

In cold water or under normal atmospheric condition, water is usually assumed to be isothermal and the sound speed for the surrounding flow is taken as a constant. The EOS for water becomes $p - p_0 = a_{\ell}^2(\rho_{\ell} - \rho_{\ell 0})$ instead of Tait's EOS, where $\rho_{\ell 0}$ is the water density at pressure p_0. Therefore, we have the following.

Corollary 3.2. *For the special case of isothermal surrounding flow, if the gas and liquid components are assumed to be isentropic and isothermal, respectively, we have*

$$\frac{\alpha}{1-\alpha} = k\frac{(p+B')/(p_{\mathrm{cav}}+B')}{(p/p_{\mathrm{cav}})^{1/\gamma}}, \tag{3.13}$$

and

$$\rho = \frac{k\rho_{\mathrm{g}}^{\mathrm{cav}} + \rho_{\ell}^{\mathrm{cav}}}{\frac{p_{\mathrm{cav}}+B'}{p+B'} + k\left(\frac{p}{p_{\mathrm{cav}}}\right)^{-1/\gamma}}, \tag{3.14}$$

where $B' = \rho_{\ell 0} a_{\ell}^2 - p_0$.

Once the density and velocity for the mixture is obtained or calculated in a conservative manner, an iteration procedure is next required to find the pressure from (3.10) to be followed by the void fraction from (3.9). Note that the latter steps do not affect the mass and momentum conservation. In general, Newton's iteration method can provide a very fast way to obtain the pressure from (3.10) given a good starting value. Due to the very low pressure inside the cavitation and the very large B, $(\bar{p}/\bar{p}_{\mathrm{cav}})^{-1/N}$ is very close to 1. Therefore, a very good starting value for the pressure iteration can be obtained as

$$p = p_{\mathrm{cav}}\left(\frac{k\rho}{k\rho_{\mathrm{g}}^{\mathrm{cav}} + \rho_{\ell}^{\mathrm{cav}} - \rho}\right)^{\gamma}. \tag{3.15}$$

Numerical tests showed that a few iteration steps could generate satisfactory results using (3.15) to provide the starting value. Furthermore, (3.15) is also a very good approximation to (3.10). One, instead, can also use it directly to obtain the pressure. During the computation, the cavitation is allowed to dynamically create and collapse based on the following principle: the flow always (starts to) cavitate whenever the liquid density is lower than ρ_{sat} and then (3.10) is used to determine the mixture pressure; the cavitating mixture changes into the pure liquid whenever the mixture density is larger than or equal to ρ_{sat} and the pressure is determined using Tait's EOS.

3.4. A procedure for determining k

In the EOS (3.10) of the present unsteady one-fluid model, k or α_0 must be somehow obtained or given. α_0, however, may not be easily obtained experimentally or otherwise for some problems due to the flow cavitating pressure being strongly related to the surrounding environment. Here we provide a simple way to obtain α_0 (or k numerically) provided p_{sat} is given. As α_0 is physically very small, k is a very small value. Under the restraint of $p \leqslant p_{\mathrm{cav}} \leqslant p_{\mathrm{sat}}$ in the cavitation region, the following condition has to be satisfied for k taken from (3.15)

$$0 < k \leqslant \frac{\rho - \rho_{\ell}^{\mathrm{cav}}}{\rho_{\mathrm{g}}^{\mathrm{cav}} - \rho}. \tag{3.16}$$

As the surrounding flow conditions are usually represented using the cavitation number, α_0 or k should therefore be closely related to the cavitation number. Similar to the definition of cavitation number for sheet/attached cavitation flow, we shall define a local cavitation number for the unsteady cavitation flow as

$$\sigma = \frac{p_{\ell\infty} - p_{\mathrm{cav}}}{0.5\rho_{\ell\infty}u_{\ell\infty}^2}. \tag{3.17}$$

Here, $(\rho_{\ell\infty}, u_{\ell\infty}, p_{\ell\infty})$ is the flow status before cavitation occurs at the flow cavitating location. Obviously, we have

$$0 < \sigma < \sigma_{\max} = p_{\ell\infty}/(0.5\rho_{\ell\infty}u_{\ell\infty}^2). \tag{3.18}$$

A small value of σ indicates a small pressure jump allowed across the cavitation interface, while a large σ imposes a large pressure jump. If k or α_0 cannot be physically determined or given beforehand, it has

to be dynamically (and artificially) determined during the computation based on the following principles:

(I) The pressure p_{cav} at the first cavitating location is determined from a given local cavitation number σ and then the initial k and α_0 are determined as discussed below.

(II) $p \leqslant p_{sat}$ is always true inside the cavitation region, where $0 < \rho < \rho_{sat}$.

Principle (I) provides a way to determine the initial k and α_0. In fact, one can also simply give k an initial value of about 0.001. This also works rather well as k is subsequently adjusted dynamically. When the liquid flow first starts to cavitate, the pressure p_{cav} at the cavitation location is obtained from (3.17) using a given cavitation number, and k can be determined from (3.10) as

$$k_{cav} = \frac{\rho_\ell^{cav} - \rho_{\ell\infty}}{\rho_{\ell\infty} - \rho_g^{cav}} \tag{3.19}$$

and the void fraction is then calculated from (3.9) or using k_{cav}. Principle (II) implies that the adjustment to k may be required because the initial k as *artificially* obtained may not be physically accurate. More specifically, because the pressure drop across the cavitation interface is relatively large in the earlier formation of cavitation (while it can be very small or even disappears in the later stages of cavitation development), k_{cav} as obtained from (3.19) may be too large such that the pressure obtained from (3.10) using k_{cav} at the newly created cavitating locations may be larger than p_{sat} during cavitation expansion. Therefore, k has to be simultaneously adjusted to a smaller value. The adjustment of k can be implemented by the following way: once pressure calculated from (3.10) is larger than p_{sat} using the initial k, k is adjusted to

$$0 < k_{new} = \beta \frac{\rho - \rho_\ell^{sat}}{\rho_g^{sat} - \rho}. \tag{3.20}$$

Here β is considered as a safety parameter smaller than but close to 1. In the present studies, it is fixed and set to 0.9. In practice, there may be many newly created cavitating locations, where the pressure, supposed to be lower than p_{sat}, is larger than p_{sat} using (3.10) with the initial k. A k_{new} is obtained using (3.20) for each location; the smallest k_{new} is used to replace the initial k and then the pressure in the cavitation region is calculated. Because the pressure decreases with the decrease of density inside the cavitation during the expansion of cavitation, the pressure obtained will always be lower than p_{sat} using the newly determined k at the existing cavitation locations. This implies that only the newly created cavitating locations are required to ascertain if the pressure is beyond p_{sat}. Numerical tests showed that only a few adjustments of k are required. Once k is adjusted to a *reasonable* value, it is fixed and applicable to the later stage of cavitation evolution including cavitation collapse. Numerical tests also showed that the final fixed k ranges between 10^{-5} to 10^{-2} depending on the surrounding flow conditions. We have carried out and evaluate the effect of two different ways to determine k or α_0; one is to fix k to a small value initially; the other is to use the more complex way as introduced above to adjust and determine it. It has been found that the selection of k affects the pressure jump magnitude across the cavitation interface but not significantly. This is because the saturate pressure p_{sat} is usually taken physically realistic to be of small magnitude to the maximum pressure in the flow field. The different selection of k does not significantly influence the cavitation dimension and cavitation collapse.

It may be reiterated, however, if α_0 can be determined experimentally or provided, the above procedure for calculating a physically feasible k becomes a non-issue.

With this proposed model, the unphysical pressure variation inside the cavitation region, which can be higher than the surrounding pressure, does not occur; the pressure inside the cavitation region will not exceed the given physical saturated pressure. In addition, one can (theoretically) apply the model to simulate attached/sheet cavitation where usually the influence of turbulence must be taken into consideration by employing the (compressible) N–S equations instead of the Euler equations given in (2.1);

this is attributed to the presence of the wake part for attached/sheet cavitation and the flow is usually turbulent. However, the discussion on the applicability and efficiency of the proposed model as applied to the compressible N–S equations is beyond the scope of the present work and will be pursued in future.

4. Applications

Besides the difficulties arising from physically modelling cavitation flow, which is the focus of the present work, there are difficulties from the numerical aspect in computing the cavitating flow. Because the coupled system of incompressible flow (the pure liquid phase) with compressible flow (the mixture) is very stiff in the vicinity of cavitation interface (boundary) in the simulation of attached/sheet cavitation, (severe) numerical instability and/or convergence problem can occur. Thus, additional numerical techniques are usually required to overcome such difficulties [16,25]. In the present study, both the surrounding medium (liquid) and the mixture are considered as compressible, the resultant system is therefore mathematically well-posed. When a high-resolution scheme developed for the compressible single phase flow is directly applied to multi-phase flow [10,17] and the present cavitating flow, the numerical oscillations may occur because of the employment of different EOS across the interface. However, such difficulties may not be so severe and overwhelming since the jumps across the cavitation interface are relatively small, and a high-resolution scheme developed for compressible single phase flow with well-designed limiter [26] can still give satisfactory results. The numerical experiments to be carried out in this section will also show that a well-developed high-resolution scheme with a compromised CFL number can prevent or greatly suppress these oscillations but may not be able to remove them completely. It is found that there is no numerical oscillation encountered using the present model with *full* CFL number in the present study except for Cases 4 and 5. Even for the latter two Cases, the present model can provide acceptable results with well-limited oscillations under the *full* CFL number. Of course, a scheme with larger CFL number without numerical oscillations associated with the present model is sought after and this is the topic for our future research.

For purpose of testing the validity of the present model, the results obtained via the Cut-off model, Vacuum model and Schmidt's model will also be presented. It should be noted that the Cut-off model and Vacuum model are pure phase models. The usual *full* CFL number at, say, 0.8 to 0.9 can be used without incurring numerical oscillations. However, the same but much lower value of CFL number valid for Schmidt's model is used throughout for all models for the purpose of direct comparison. The Vacuum model developed in [27] has been shown to be reasonable both mathematically and physically except for the difficulties in extending to multi-dimensions. Wherever possible, the analytical solution based on the Vacuum model for one dimension will be employed to verify the numerical results of the present model. As analysed in Section 3.2, there are inherent numerical oscillations present using Schmidt's model due to p'_{sat} far larger than p_{sat}, whenever the surrounding pressure is developed to be lower than p'_{sat} with the expansion of cavitation extent. It is found, however, that the oscillations generated in the cavitation expansion phase can be made well limited under a small CFL number and even mitigated when the surrounding pressure exceeds p'_{sat} during the cavitation contraction phase. In general, to obtain results with well-limited oscillations using Schmidt's model for the various Cases in the present study, a much smaller CFL number is required in comparison to the present model. A smaller than the usual intended CFL number (which is typically about 0.8 to 0.9) found applicable for Schmidt's model is, therefore, used for all the models in the calculations. Had a larger CFL number, say, applicable to the present model been employed, it would usually lead to even more severe oscillations for Schmidt's model and in some cases invalid results such as Cases 4 and 5 to be discussed below. The present study suggests that Schmidt's model may be applied to problems, where cavitation can evolve to a larger size but with inherent oscillations and much restraint placed on the CFL number employed. After the cavitation collapses, the flow returns to pure liquid phase;

the restraints imposed on the CFL number are then relaxed and it has been found that the oscillations generated in the cavitation expansion stage can even disappear.

The numerical scheme selected and used to solve system (2.1) is the well-developed HLL [13] scheme. The detailed discussion about this scheme can be found in [28]. In this section, the present model will be tested and verified by either comparing to the *analytical* solution, experiments or numerical results. After the comparison, the present model is then applied to a 3D underwater explosion in a cylindrically symmetric container, similar to the work done in [33]. As α_0 is unknown for each problem to be discussed in the tests, we use the procedure developed in Section 3.4 to determine α_0 and adjustment made to k accordingly. In the present computation, p_{sat} is set to 22.0 Pa and the local cavitation number σ is set to $0.1\sigma_{\max}$ in the computation of the initial k for the present model unless otherwise noted. In the use of Schmidt's model, p'_{sat} is calculated and assumes the value of 1.55 kPa.

Case 1 (*1D cavitating flow in an open tube in high pressure*). This is a Riemann problem of two highly pressurised water streams moving with the same magnitude of velocity in the opposite direction away from the centre of a tube. The initial pressure of the two water streams is set to 1000 bar. The computational domain is $[0, 1m]$. The two water streams initially meet at $x = 0.5$ m and the CFL number is set to 0.5 over 400 uniform mesh. If the magnitude of the initial two-water stream velocity is not sufficiently high, two opposite centred rarefaction waves are generated and expand from the centre. In such a situation, exact solution can be obtained by solving a Riemann problem of double rarefaction waves. The present model and the associated codes can automatically treat the flow as single phase. Fig. 1 shows the velocity result obtained by the present model for a velocity magnitude of two streams initially set to 50 m/s and compared well to the analytical solution at 0.2 ms. If the initial velocity magnitude of two water streams is beyond a critical value (which can be determined theoretically), cavitation immediately starts at the centre. The *exact* solution can also be obtained by solving a Riemann problem of double rarefaction waves connected to a vacuum at the centre [27] (i.e. the exact solution based on the Vacuum model for this problem). Due to p_{sat} set to be negligibly small physically at least relative to the initial very high surrounding pressure, the results

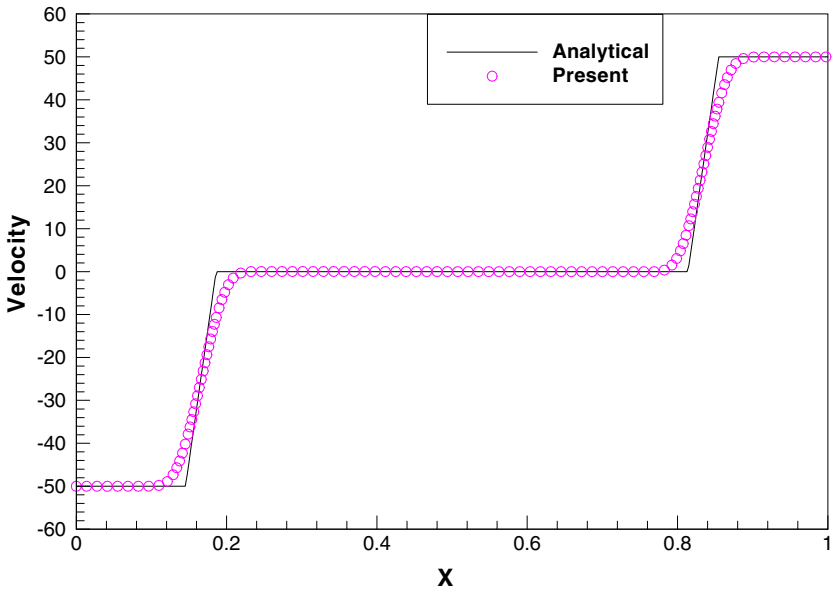

Fig. 1. The comparison of velocity profile by the present model to the analytical solution for Case 1 with a velocity magnitude of 50 m/s at 0.2 ms.

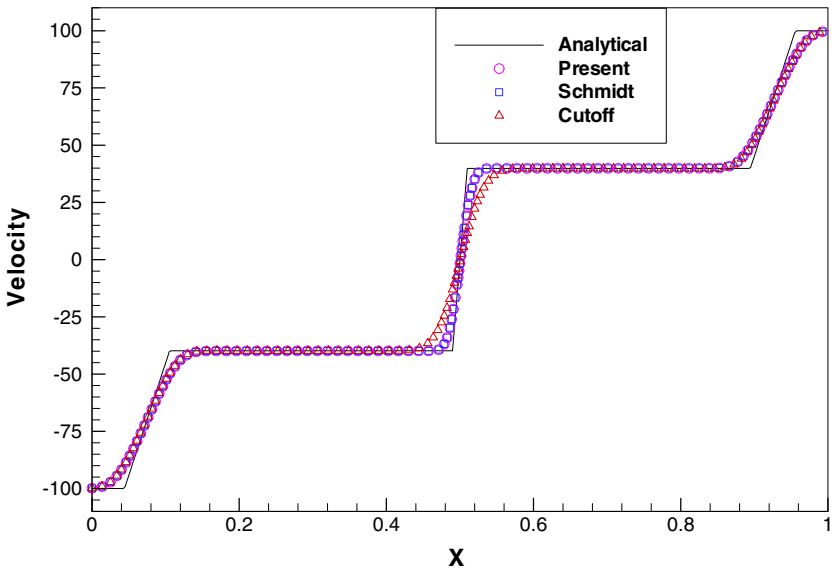

Fig. 2. The comparison of velocity profile by the present model to the analytical solution, the Cut-off model and Schmidt's model for Case 1 with a velocity magnitude of 100 m/s at 0.25 ms.

provided by the present model can be directly compared to the exact solution of the Vacuum model. Fig. 2 shows the velocity profiles obtained by the present model, the Cut-off model and Schmidt's model for an initial velocity magnitude set to 100 m/s at time $t = 0.25$ ms. It is observed from Fig. 2 that the three models provide the same results in the region beyond the cavitation. In particular, the Cut-off provides a result with a larger cavitation dimension, while the present model and Schmidt's model provide results very close to the analytical solution in this very earlier stage. Note that, however, as time progresses, numerical oscillations occur for Schmidt's model; the oscillations become severe with the increase of CFL number and can even cause computation difficulties. The present model still works very well even when the CFL number is set to

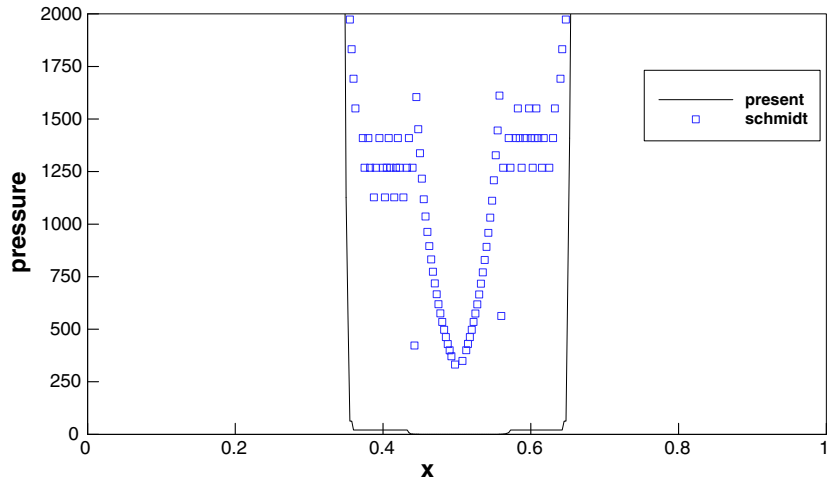

Fig. 3. The close-up view of pressure profiles provided by the present model and Schmidt's model for Case 1 with a velocity magnitude of 100 m/s at 0.1 ms and CFL = 0.9.

0.9. Fig. 3 shows the close-up view of pressure profiles in the cavitation region obtained with CFL = 0.9 at $t = 0.1$ ms using the present model and Schmidt's model, respectively. In Fig. 3, the pressure inside the cavitation is apparently higher than the surrounding pressure in the vicinity of the cavitation interface, resulting in numerical oscillations observed in the liquid. There is no oscillation observed for the present model. One may also observe that there is a small pressure jump across the cavitation interface as analysed in Section 2.2.

Case 2 (*1D cavitating flow in an open tube in one atmosphere*). This is also a problem of two water streams moving with a velocity magnitude of 100 m/s in the opposite direction from the centre of a tube at one atmosphere. The computational domain is the same as Case 1. This case was previously investigated by Saurel and Abgrall [23] using Saurel's multiphase model comprising seven governing equations. A uniform mesh of 400 cells is used and the CFL number is set to 0.5.

The results of velocity profiles at five different instances of 0.5, 1.0, 1.5, 2.0 and 2.5 ms obtained by the present model are shown in Fig. 4. These are very comparable to Saurel and Abgrall [23]. Fig. 5 shows the comparison of the results obtained respectively by the present model, Schmidt's model and the Cut-off model at 0.2 ms. The results between the present model and Schmidt's model look very similar, while obvious discrepancies in the density and velocity profiles can be observed for the Cut-off model. An almost twice the cavitation size is provided by the latter in contrast to that provided by the former two models (see density profile in Fig. 5(a)). The lowest density obtained by the latter is also doubly higher than those provided by the former two models. The pressure profiles shown in Fig. 5(b) indicate minimal difference among the three models outside the cavitation region except that Schmidt's model provides slightly higher pressure there due to the large p'_{sat}. On the other hand, if we look closely at the inside of the cavitation region, essential differences among three models are again clearly exhibited. (In Figs. 6(a)–(c) showing the pressure distribution at the same time $t = 0.2$ ms, the embedded small figures within each series depict the closed-up behaviour in the cavitation region.) A pressure jump across the cavitation boundary is clearly captured by the present model and the cavitation range is from 0.39 to 0.61 (see Fig. 6(a)). Beside the pressure jump across the cavitation interface, there are apparent numerical oscillations observed across the cavitation interface using Schmidt's model (Fig. 6(b)). Again, a larger CFL employed leads to much severe oscillation for the Schmidt model, while the present model still works well even with CFL set to 0.9 for this problem. Without additional treatment, these pressure oscillations can disperse and even cause computational difficulties during the expansion of cavitation. The cavitation range captured by Schmidt's mode is from 0.41 to 0.59. Using the Cut-off model the pressure jump across the cavitation interface is initially through one step. With the further expansion of cavitation, two or more steps of small jumps may be observed. This is probably due to the inconsistency occurring between the sound speed used and the EOS

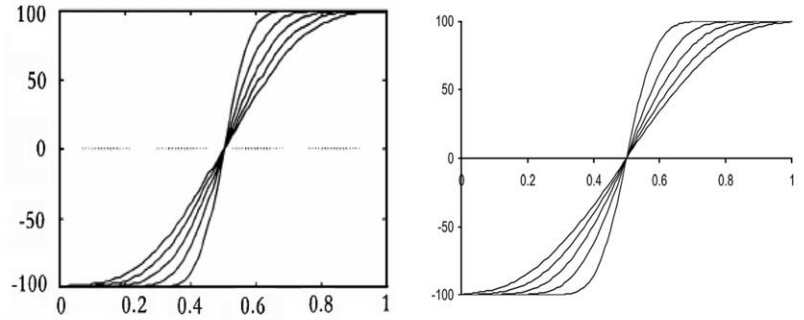

Fig. 4. Comparison of velocity profiles at the various times of 0.5, 1.0, 1.5, 2.0, and 2.5 ms between Saurel's multiphase model (left) (duplicated from [22]) and the present model (right) (Case 2).

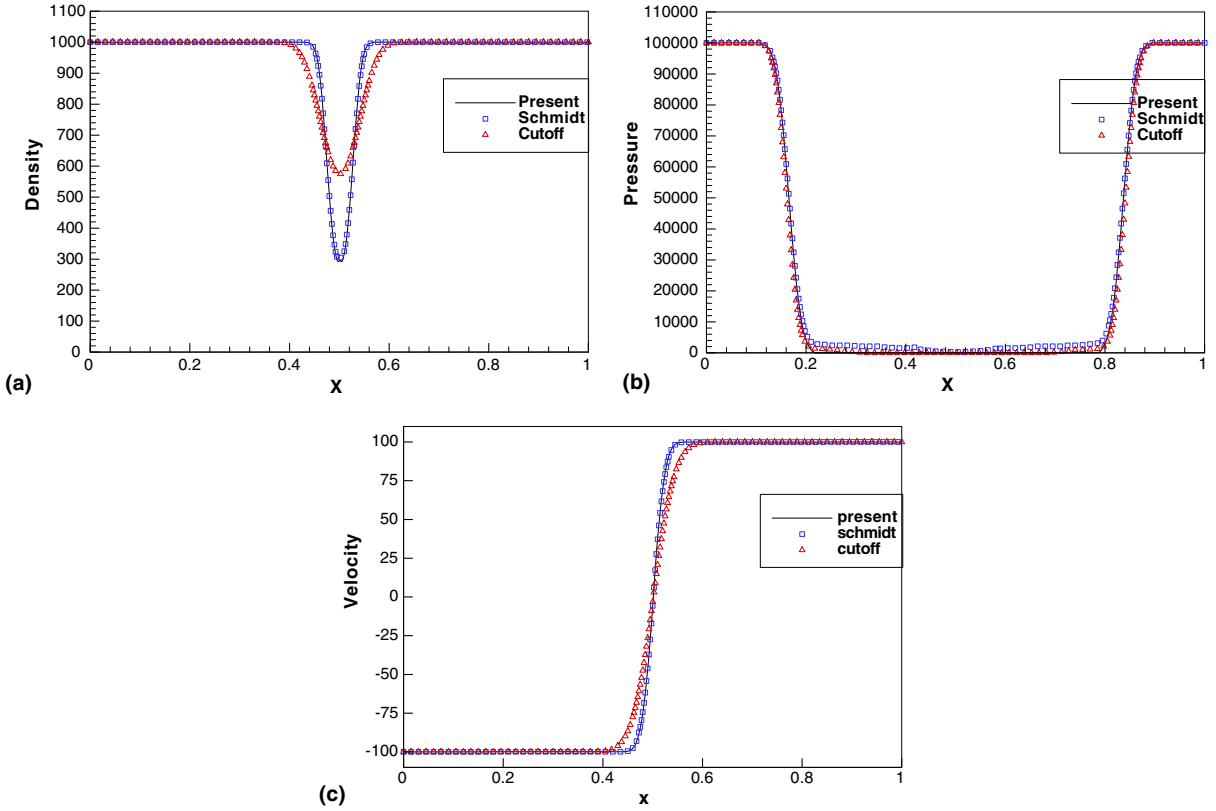

Fig. 5. Comparison of the three models at $t = 0.20$ ms (Case 2).

(3.1) as discussed in Section 3.1. The cavitation range captured by the Cut-off model is from 0.31 to 0.69. This implies that the Cut-off model provides a much faster expansion speed of cavitation among the three models.

Case 3 (*1D cavitating flow in a closed tube*). This case is similar to Case 2, except that the two ends of the tube are simultaneously closed once the flow starts. Therefore, a shock created at each end moves towards the centre, resulting in shock–cavitation interaction and cavitation collapse. The flow initial status and computational conditions are kept the same as for Case 2; the CFL number is set to 0.5. The walls at the two ends are treated as reflective boundaries. The purpose of this problem is to study the shock–cavitation interaction and cavitation collapse. In this problem, the flow is initially pure water and soon changes phase into a vapour–water mixture at the centre, and then reverting back into a pure liquid after the cavitation collapse. Figs. 7 and 8 depict a series of plots for the three models at the time instance of 0.3 and 0.5 ms, respectively. The results between the present model and Schmidt's model are close to each other during the whole computation for this problem except for the differences as observed and discussed in Case 2 during the cavitation expansion. The results provided by the Cut-off model, however, are very different from those provided by the former two models. It is observed that the shocks created at the ends propagate towards the centre and meet the outward propagating rarefaction generated at the centre. The shock then propagates through the rarefaction region with a mitigated strength and then interacts with the expanding cavitation interface. As a result, a stronger discontinuity forms at the cavitation interface, where a larger pressure and

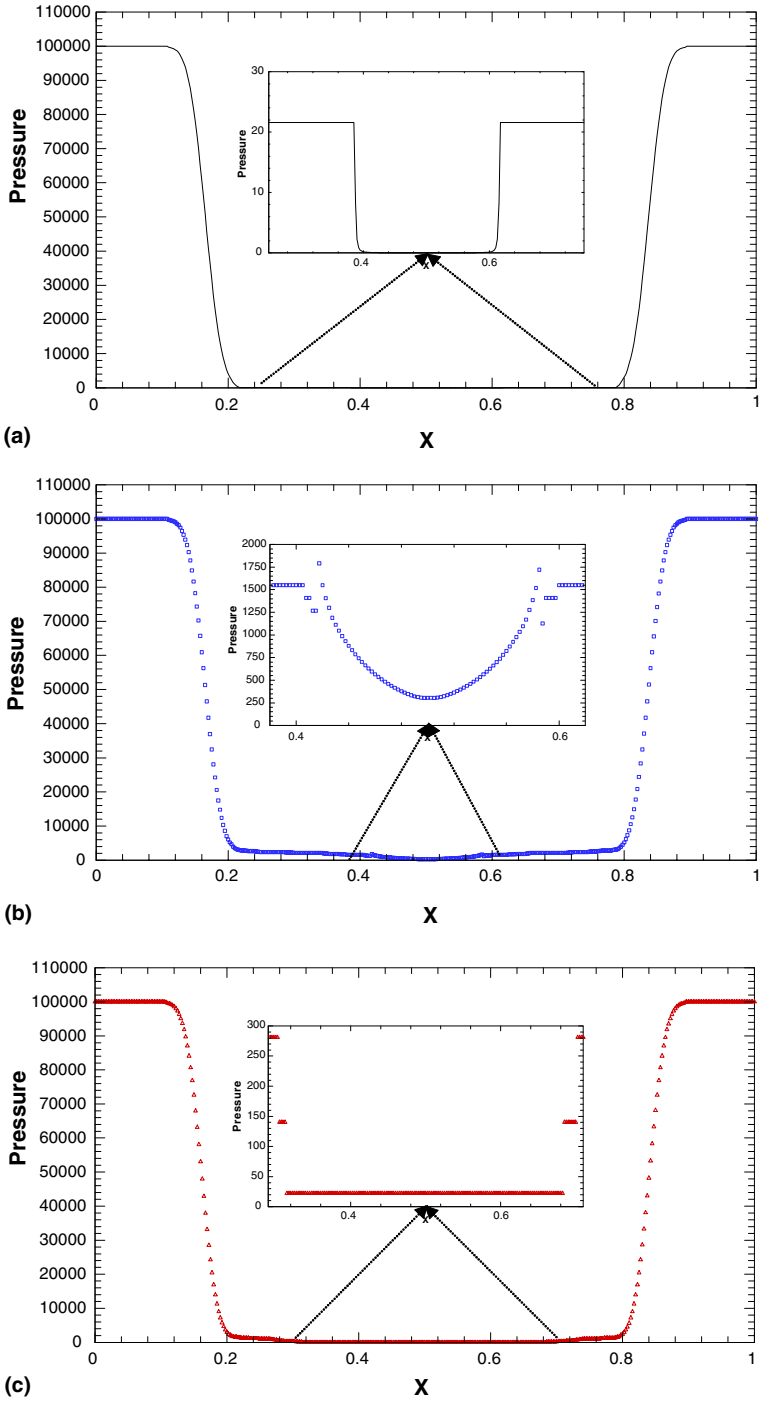

Fig. 6. (a) The present model at $t = 0.2$ ms (Case 2). (b) Schmidt's model at $t = 0.2$ ms (Case 2). (c) The Cut-off model at $t = 0.2$ ms (Case 2).

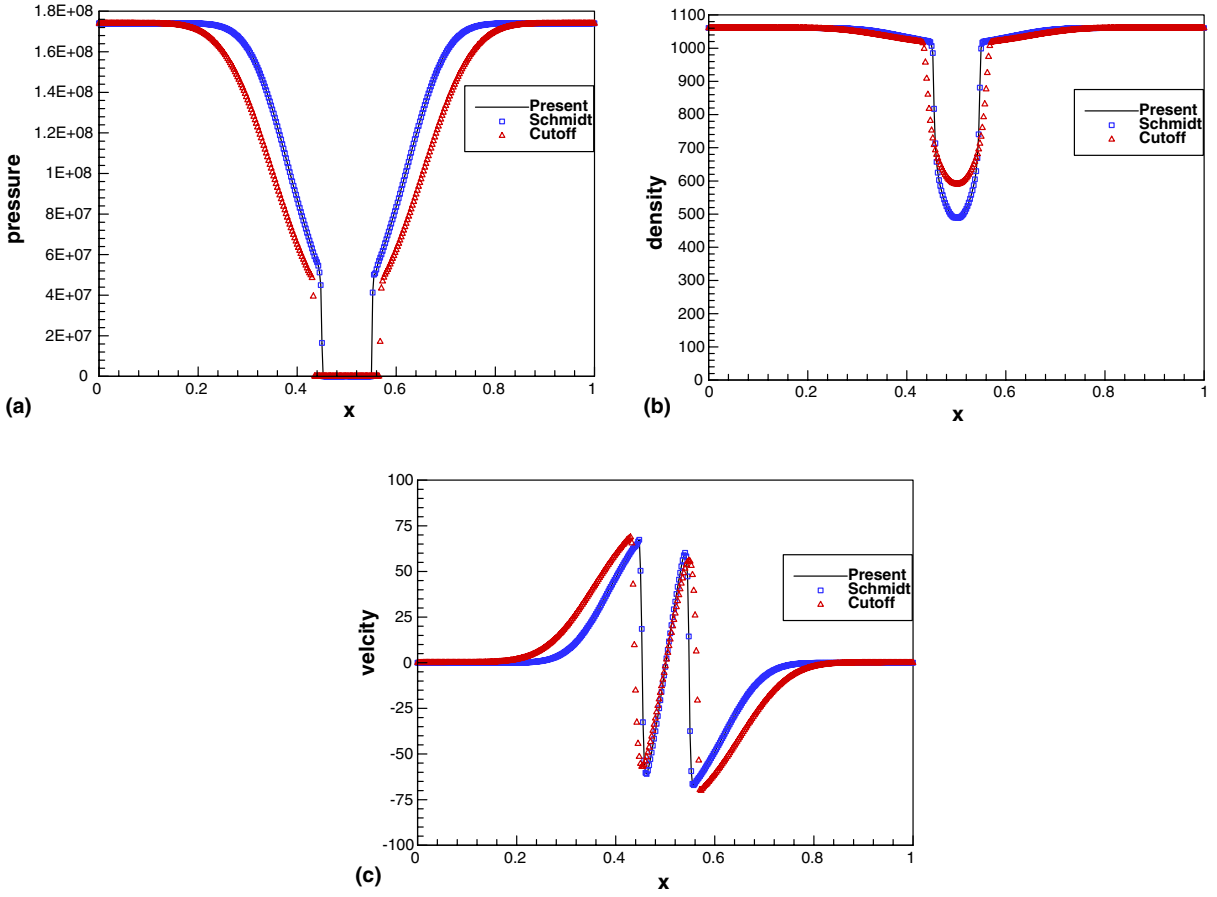

Fig. 7. The flow at $t = 0.3$ ms just before cavitation collapse (Case 3).

velocity jump occurs. This leads to the cavitation interface moving like a "genuine shock" and the beginning of cavitation collapse. The plots shown in Fig. 7 are the results just before the cavitation collapse, while the plots in Fig. 8 are the results after cavitation collapse. After the cavitation collapse, the flow changes back into a pure liquid. The numerical oscillations occurring during cavitation expansion for Schmidt's model then gradually disappear. The cavitation collapse generates two shocks which propagate outwards with equal strength as that for the shocks generated initially at the two ends. The Cut-off model provided a larger dimension of cavitation, resulting in a far later cavitation collapse for this problem. Again, the present model works well for CFL set to 0.9, while computation difficulties are encountered for Schmidt's model.

Case 4 (*1D gas–water shock tube problem in a closed tube*). This case is taken from Tang and Huang [27]. In their work, a vacuum model was developed and employed. The tube is occupied by a highly pressurised gas on the left and low-pressure water on the right, and the length of tube occupied by the gas is much smaller than that by the water. The initial conditions are $\rho_L = 70.735$ kg/m^3, $p_L = 100692985.3$ Pa, $u_L = 0.0$, $\gamma_L = 2.0$, $(x < 0.001)$; $\rho_R = 1000$ kg/m^3, $p_R = 101325$ Pa, $u_R = 0.0$, $\gamma_R = 7.15$, $(0.001 \leqslant x < 0.275)$. A uniform mesh of 1100 cells is used and the CFL number is set to 0.1, which is nearly the maximum workable

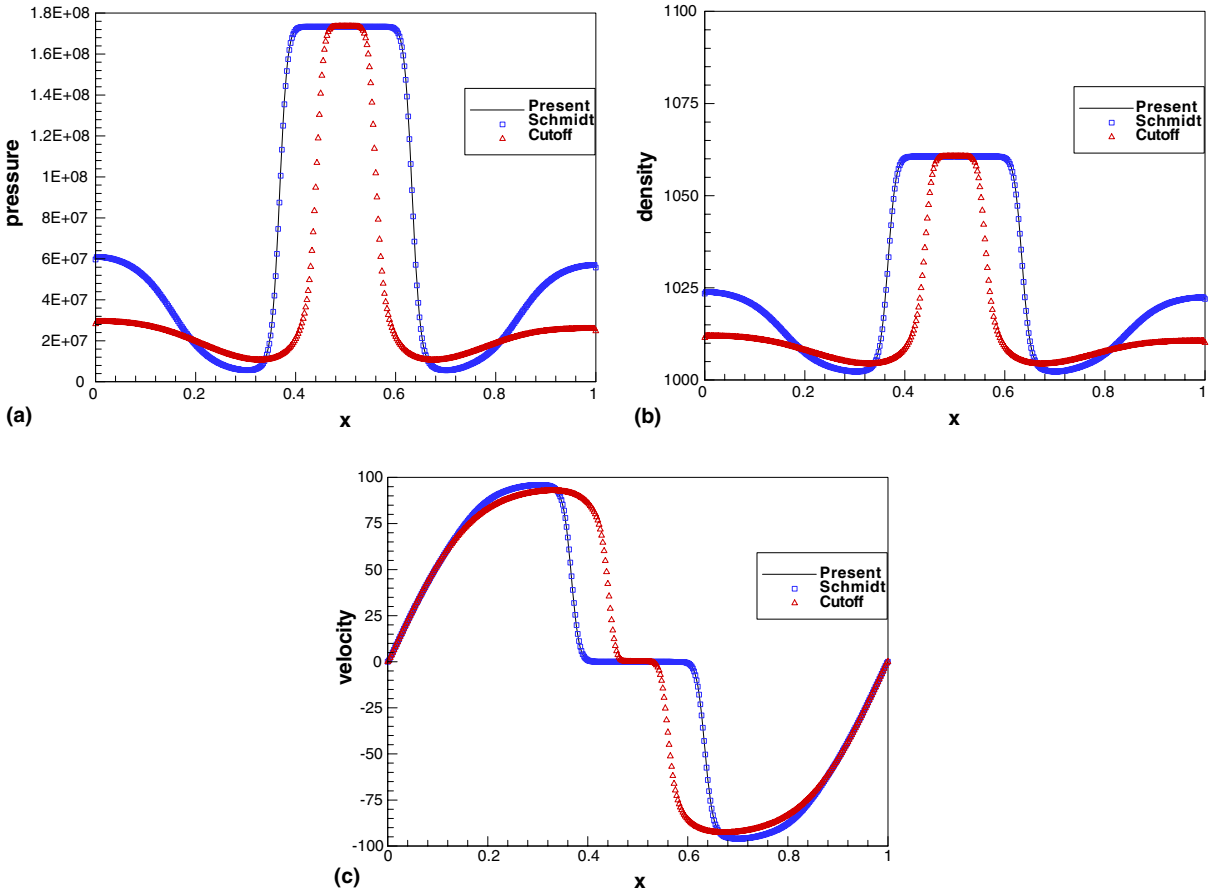

Fig. 8. The flow after cavitation collapse at 0.5 ms (Case 3).

CFL for Schmidt's model for this problem. The explosive gas–water interface is treated with the Ghost Fluid Method technique developed in [20]. One purpose of this study is to analyze the shock–cavitation–structure interaction. After the diaphragm separating the explosive gas and water is removed, a strong shock is generated and propagates in the water and a strong rarefaction wave simultaneously propagates towards the left end. With time, the shock impacts the right-end wall and is then reflected. The reflected shock wave from the right end meets and goes through the reflected rarefaction from the left wall with a slightly mitigated strength and finally impacts the explosive gas–water interface, resulting in a relatively weak shock transmitted into the explosive gas and a relatively very strong rarefaction wave back into water, which leads to the creation of a cavitation region next to the interface. The cavitation right boundary moves with a speed faster than the local flow velocity and rapidly expands towards the right. Simultaneously, the reflection of the transmitted shock wave from the left wall soon propagates through the interface and interacts with the left expanding cavitation boundary. Such shock–cavitation interaction causes the left cavitation boundary to move also towards the right with an enhanced pressure jump. As a result, the whole cavitation region moves towards the right with an expansion at the right side and collapse at the left side. With the left cavitation boundary impacting on the right wall, the cavitation finally collapses at the right end, resulting in a strong shock generated and which propagates towards the left. Similar cavitation cre-

ation and collapse subsequently occur many times. Fig. 9(b) shows the pressure history at the right end obtained with the present model, the Cut-off model and Schmidt's model. Among the three models, the respective pressure history curves looks very similar. The result by the Vacuum model is reproduced in Fig. 9(a) for comparison. The comparison looks reasonable except for the smaller initial peak pressure as registered by the Vacuum model. This is possibly due to less grid points used in [27]. Although the curves of pressure history in Fig. 9(b) indicate no significant difference, there are obvious differences between the detailed flow fields during the cavitation collapse. Fig. 10 shows the pressure profiles provided by the three models just before the first cavitation collapses. The present model and Schmidt's model provide very similar results, while there is relatively flatter pressure profile provided by the Cut-off model. The magnitude of pressure jump across the cavitation interface and the location of cavitation boundary captured among the three models, however, are very similar for this problem. This is possibly one reason the Cut-off is able to provide reasonable end pressure history for this specific problem.

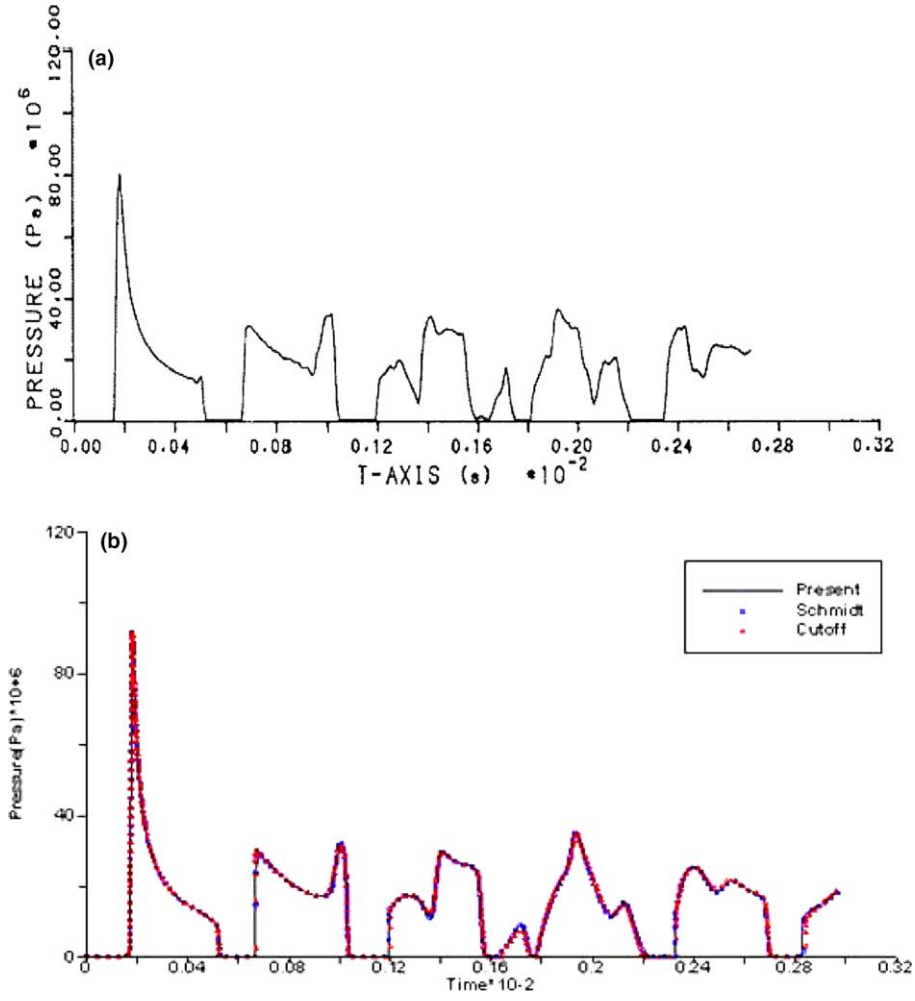

Fig. 9. Pressure history at the right end wall: (a) numerical simulation by vacuum model ($P_v = 0$); (b) numerical simulation by three different models (Case 4).

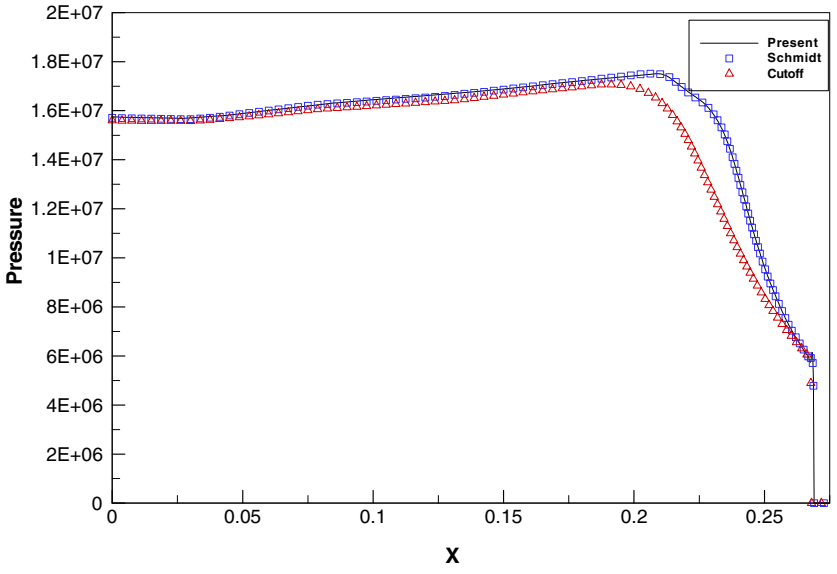

Fig. 10. Pressure profile at $t = 0.00065$ s by three models (Case 4).

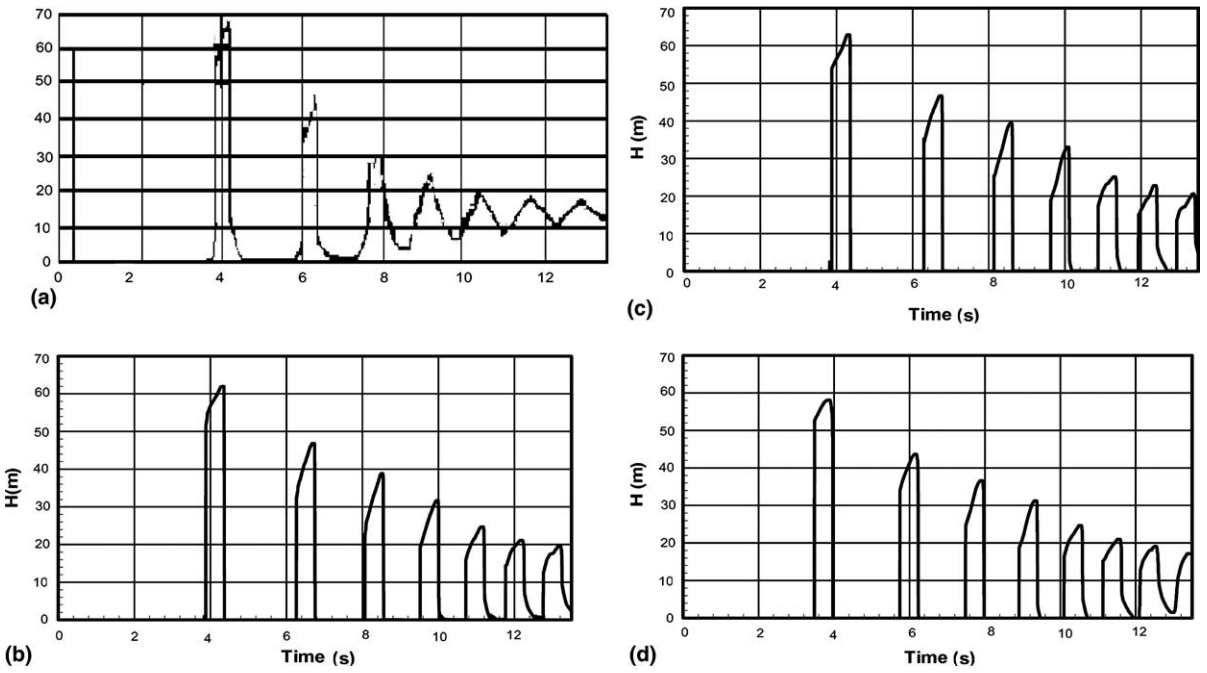

Fig. 11. Pressure history at upstream end: (a) experimental results (duplicated from [21]); (b) the present model; (c) Schmidt's model; (d) the Cut–off model (Case 5).

Case 5 (*1D water hammer problem*). A long water pipe with a valve on the left is connected to a reservoir on the right. When the valve is suddenly closed, a cavitation is created next to the valve and the well-known water hammer phenomenon is then observed. This problem involves cavitation–structure interaction. To facilitate comparison, the case study in [22] is selected, where experimental data are available under isothermal condition. A source term $S = [0, -f\rho u|u|/2D]^{\mathrm{T}}$ is added to (2.1) in order to account for the viscous friction. Here, f is the Darcy friction factor and D is the diameter of the pipe. We use the same flow conditions as presented in [22] and carry out the simulation under isothermal condition by employing EOS (3.14) developed in Section 3.3. The initial states are given as follows: the upstream pressure at the inlet is 5.49164 bar and downstream pressure at the reservoir is 0.98065 bar. The water density is 1000 kg/m^3 and the fluid flows at a constant speed of 1.5 m/s before the valve is closed. From the given conditions, it can be deduced that $f/D = 2.0\ \mathrm{m}^{-1}$ and the constant B' appearing in EOS (3.14) is 6.723E8Pa. A uniform mesh of 1000 cells is used for the calculation. The left end is treated using the reflective boundary condition, while the right end is imposed the reservoir condition. The CFL number is set to 0.1 in order that Schmidt's model is able to provide reasonable results for purpose of comparison to the present model. Figs. 11(b)–(d) show the pressure history at the valve obtained by the present isothermal model, Schmidt's model and the Cut-off model, respectively, together with the experimental result provided in Fig. 11(a). It is found that the present model and Schmidt's model provide first cavitation collapse pressure head of about 62 and 63 m, respectively, which is very close to the experimental result of 66 m, while the Cut-off model provides the first pressure surge of 58 m. It is also interesting to note that the present model predicted very similar periods of cavitation collapse as compared to the experiments. There is one more collapse cycle as obtained by the Cut-off model for the time interval of 14s, while Schmidt's model indicates a slightly larger period between the pressure surges. Again, much severe oscillations can appear with the increase of CFL number. For example, Fig. 12 shows the pressure profiles obtained by the three models with CFL = 0.8 at the time of 0.925 ms. Far more severe oscillations are observed for Schmidt's model in comparison to the present model. There are several other similar water hammer experiments carried out in [22], and the present developed isothermal model(3.14) has successfully reproduced all those experimental results (not shown).

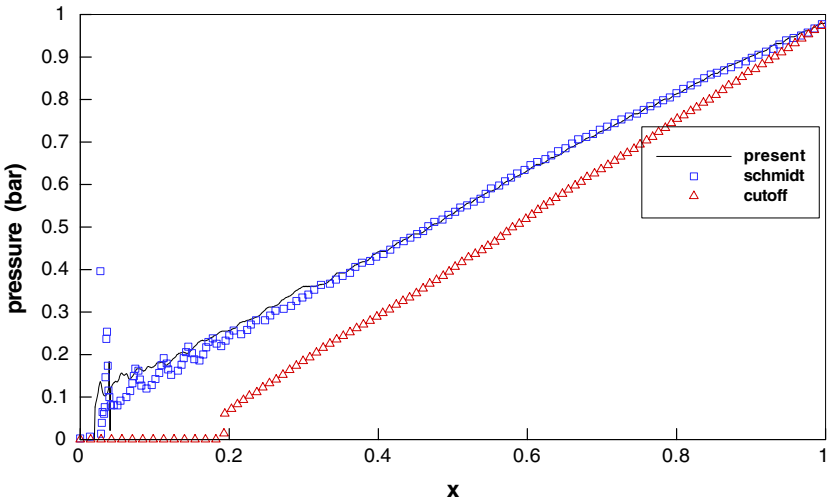

Fig. 12. The pressure profiles provided by the three models before first cavitation collapse (Case 5).

Case 6 (*A spherical underwater explosion in a rigid cylindrical container*). The diameter and height of the cylinder are 0.0889 and 0.2286 m, respectively. The explosive gas sphere is located at the centre of the cylinder full of water. The diameter of the gas sphere is 0.03 m. The initial pressure and density inside the gas sphere are 20,000 bar and 1770 kg/m^3. γ is set to 2 for the explosive gas. There are 71×361 grid-points uniformly distributed for the meridian plane domain since the problem is cast into a 2D cylindrical coordinate system. The p_{sat} is set to 0.05 bar. The CFL number is set to a relatively large value of 0.45. It is interesting to note that there is no non-physical oscillation encountered for Schmidt's model for this problem. This is because the cylinder size is relatively small and the initial flow is under very high pressure condition; Schmidt's model has no difficulty when applied in such a small-size, high pressure situation as verified by Schmidt et al. [26]. The cylinder walls are treated using reflective boundary condition. The present study exhibits all the major complex flow physics as discussed in [33]. In [33], the experimental explosion was initiated by PETN explosive in a deformable cylinder; in their simulation, water was modeled using a polynomial EOS, where pressure cut-off was employed when the pressure was detected to be lower than the given vapour pressure. Once the explosion is initiated, a strong spherical shock is generated and propagates symmetrically outwards with an exponentially decaying strength. The reflected shock from the container side wall with a decreasing strength hits the expanding explosion bubble, resulting in a rarefaction wave reflected from the gas bubble surface [18]. The rarefaction wave can be so strong such that cavitation may be created next to the bubble surface. The rarefaction wave also makes a reflection at the cylinder side wall and then cavitation is created next to the wall. The cavitation subsequently collapses due to the compression from compressive wave, which is generated by the wave–bubble surface interaction [18]. Fig. 13 shows a series of pressure contours at the respective times of 30, 60, 90 and 120 μs. At $t = 30$ s, the underwater shock has already reflected from the cylinder wall, and the reflected shock wave has interacted with the expanding bubble surface. A rarefaction wave is generated due to the shock–bubble interaction and a low pressure region is created next to the bubble surface. At $t = 60$ μs, a large size cavitation region has been created next to the wall. The reflected shock waves from the top/bottom of the cylinder interact with those reflected from the side

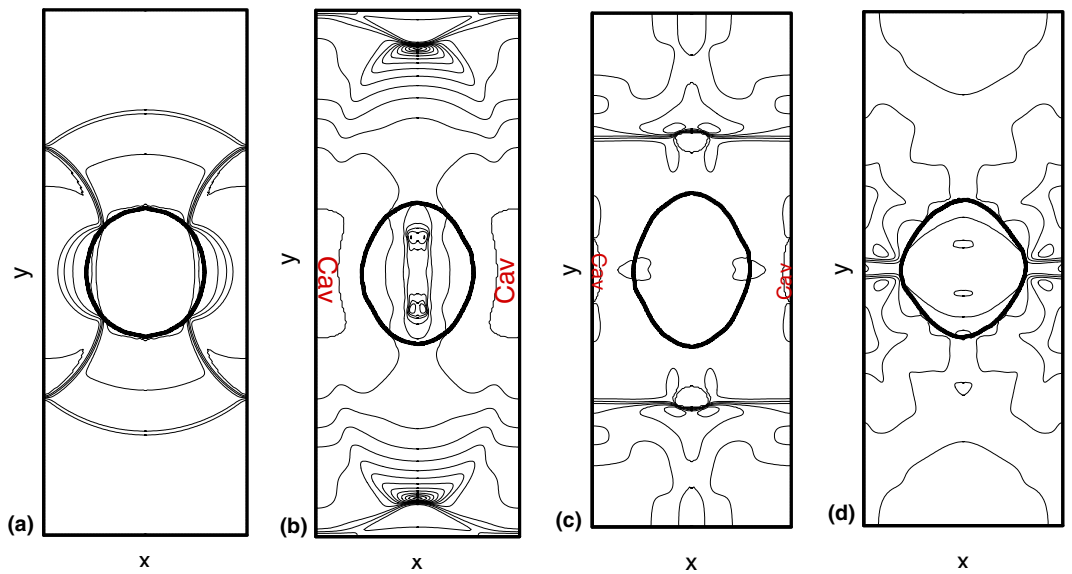

Fig. 13. Pressure contours at: (a) $t = 30$ μs; (b) $t = 60$ μs; (c) $t = 90$ μs; (d) $t = 120$ μs (Case 6). "cav" indicates the cavitation region.

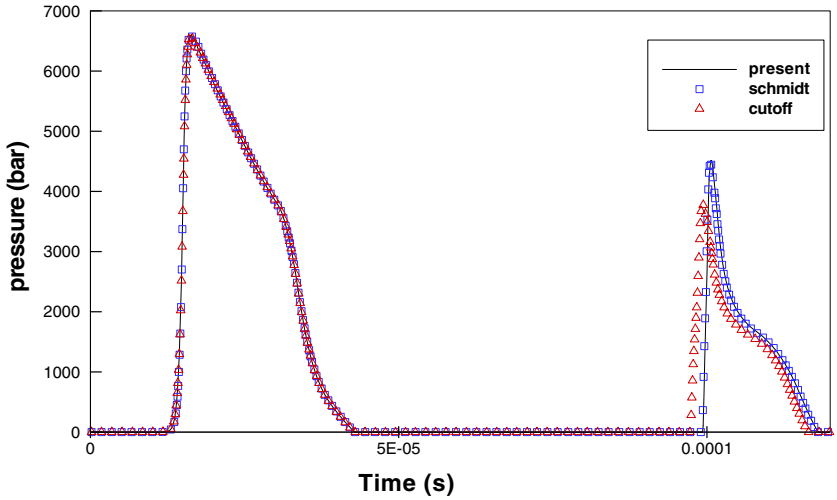

Fig. 14. Pressure history at the centre location of the side wall (Case 6).

walls, resulting in a complicated shock–shock interaction. The transmitted shocks of the reflected shock waves from the side wall inside the gas bubble have already made reflection at the gas bubble surface and caused shock focusing on two points inside the oval shaped bubble. At $t = 90$ μs, with the decrease of shock strength, the shock–shock interaction results in two nearly plane shocks propagating towards the bubble from the top and bottom. The cavitation next to the side walls is shrinking and on the verge of going to collapse. At $t = 120$ μs, the cavitation has collapsed and the resultant flow field becomes very complicated. For this problem, the Cut-off model and Schmidt's model provide fairly similar gross features as those obtained by the present model. Fig. 14 shows the pressure history at the centre point of the cylinder side wall up to 120 μs. It can be observed that the pressure histories provided by the respective three models are almost the same before the cavitation collapse. The Cut-off model provided a later cavitation collapse and a lower pressure surge, while the present model and Schmidt's model provided similar results.

5. Conclusions

Based on the assumption of homogeneous mixture of consisting of isentropic gas and liquid components, a one-fluid cavitation model has been developed for the unsteady cavitating flow, where the cavitation development is sustained mainly through pressure jump across the cavitation interface. Unlike the existing one-fluid models as discussed in this work, where the EOS for the mixture is usually inconsistent with the sound speed formulation, the present model is mathematically sound and physically reasonable. The present model has been tested and verified by comparing to either analytical solution, experiments or other numerical results and is very easy to extend and apply to multi-dimensions with no restraints placed on the cavitation dimensions.

Appendix A

This is the proof for Corollary 2.5. Using (a) and (b) and Tait's EOS, we have:

$$\rho_\ell^{\mathrm{I}}(v_\ell^{\mathrm{I}})^2 + p_\ell^{\mathrm{I}} = \rho_\ell^{\mathrm{I}}(v_\ell^{\mathrm{I}})^2 \left(\frac{\bar{p}_\ell^c}{\bar{p}_\ell^{\mathrm{I}}}\right)^{-1/N} + p_\ell^c \tag{A.1}$$

To prove Corollary 2.5, one only needs to show that equality (A.1) has no root satisfying $p_\ell^{\mathrm{sat}} \leqslant p_\ell^c < p_\ell^{\mathrm{I}}$. We note that the following function $f(p)$

$$f(p) = \rho_\ell^{\mathrm{I}}(v_\ell^{\mathrm{I}})^2 \left(\frac{\bar{p}}{\bar{p}_\ell^{\mathrm{I}}}\right)^{-1/N} + p - \rho_\ell^{\mathrm{I}}(v_\ell^{\mathrm{I}})^2 - p_\ell^{\mathrm{I}} \tag{A.2}$$

has only one extreme, which is a minimum, located at

$$\left(\frac{\bar{p}_*}{\bar{p}_\ell^{\mathrm{I}}}\right)^{1+1/N} = (M_\ell^{\mathrm{I}})^2. \tag{A.3}$$

Thus, there are at most two roots for (A.2) located in the intervals of $(-\infty, p_*)$ and (p_*, ∞), respectively. One of them is p_ℓ^{I}. Hence the proof of Corollary 2.5 is equivalent to showing that f is monotonous in $(0, p_*)$, and f (0) and (fp_*) have the same sign. The former condition is obviously held, as f is smooth and has only one extreme. As for the latter conditions, we have $f(0) = N\bar{p}_\ell^{\mathrm{I}}(M_\ell^{\mathrm{I}})^2[(\bar{p}_\ell^{\mathrm{I}}/\bar{B})^{1/N} - 1] - p_\ell^{\mathrm{I}}$. Because $(\bar{p}_\ell^{\mathrm{I}}/\bar{B})^{1/N} - 1 < p_\ell^{\mathrm{I}}/N\bar{B}$, it is easy to check that $f(0) < 0$ with the given condition. Solving (A.3) for p_* and substituting it into (A.2), one obtains

$$f(p_*) = \bar{p}_\ell^{\mathrm{I}}\{N(M_\ell^{\mathrm{I}})^2[(M_\ell^{\mathrm{I}})^{-1/(N+1)} - 1] + (M_\ell^{\mathrm{I}})^{2N/(N+1)} - 1\}. \tag{A.4}$$

It can be shown that for any $0 < M_\ell^{\mathrm{I}} < 1$, $f(p_*) < 0$. This concludes the proof. □

References

[1] J.E. Aanhold, G.J. Meijer, P.P.M. Lemmen, Underwater shock response analysis on a floating vessel, Shock Vibr. 5 (1998) 53–59.
[2] V. Ahuja, A. Hosangadi, S. Arunajatesan, Simulation of cavitation flows using hybrid unstructured meshes, J. Fluid Eng. 123 (2001) 331–340.
[3] G. Allaire, S. Clerc, S. Kokh, A five-equation model for the simulation of interfaces between compressible fluids, J. Comput. Phys. 181 (2002) 577–616.
[4] C.E. Brennen, Cavitation and Bubble Dynamics, Oxford University Press, Oxford, 1995.
[5] Y. Chen, S.D. Heister, A numerical treatment for attached cavitation, J. Fluid Eng. 116 (1994) 613–618.
[6] Delannoy, J.L. Kueny, Two phase flow approach in unsteady cavitation modelling, Cavitation Multiphase Flow Forum, FED 98 (1990) 152–158.
[7] M. Deshpande, J. Feng, C.L. Merkle, Cavity flow predictions based on the Euler equations, J. Fluid Eng. 116 (1994) 36–44.
[8] M. Deshpande, J. Feng, C.L. Merkle, Numerical modeling of the thermodynamic effects of cavitation, J. Fluid Eng. 119 (1997) 420–427.
[9] S. Evje, K.K. Fjelde, Hybrid flux-splitting schemes for a two-phase flow model, J. Comput. Phys. 175 (2002) 674–701.
[10] R.P. Fedkiw, A. Marquina, B. Merriman, A non oscillatory Eulerian approach to interfaces in multimaterial flows (the ghost fluid method), J. Comput. Phys. 152 (1999) 457–492.
[11] S. Gavrilyuk, R. Saurel, Mathematical and numerical modeling of two-phase compressible flows with micro-inertia, J. Comput. Phys. 175 (2002) 326–360.
[12] I.I. Glass, J.P. Sislian, Nonstationary Flows and Shock Waves, Oxford Science Publication, 1994.
[13] A. Harten, P.D. Lax, van B. Leer, On upstream differencing and Godunov type schemes for hyperbolic conservation laws, SIAM Rev. 25 (1983) 33–61.
[14] D. Jamet, O. Lebaigue, N. Coutris, J.M. Delhaye, The second gradient method for the direct numerical simulation of liquid–vapour flows with phase change, J. Comput. Phys. 169 (2001) 624–651.
[15] A. Kubota, H. Kato, H. Yamaguchi, A new modelling of cavitating flows: a numerical study of unsteady cavitation on a hydrofoil section, J. Fluid Mech. 240 (1992) 59–96.

[16] R.F. Kunz, D.A. Boger, D.R. Stinebring, T.S. Chyczewski, J.W. Lindau, H.J. Gibeling, S. Venkateswaran, T.R. Govindan, A preconditioned Navier–Stokes method for two-phase flows with application to cavitation prediction, Comp. Fluids 29 (2000) 849–875.
[17] T.G. Liu, B.C. Khoo, K.S. Yeo, The simulation of compressible multi-medium flow. Part I: a new methodology with test applications to 1D gas–gas and gas–water cases, Comp. Fluids 30 (3) (2001) 291–314.
[18] T.G. Liu, B.C. Khoo, K.S. Yeo, The simulation of compressible multi-medium flow. Part II: applications to 2D underwater shock refraction, Comp. Fluids 30 (3) (2001) 315–337.
[19] T.G. Liu, B.C. Khoo, K.S. Yeo, C. Wang, Underwater shock-free surface–structure interaction, Int. J. Numer. Meth. Eng. 58 (4) (2003) 609–630.
[20] T.G. Liu, B.C. Khoo, K.S. Yeo, Ghost Fluid Method for strong shock impacting on material interface, J. Comput. Phys. 190 (2003) 651–681.
[21] J.R. Qin, S.T.J. Yu, M.-C. Lai, Direct calculations of cavitating flows in fuel delivery pipe by the Space–Time CE/SE method, Society of Automotive Engineer, 1999-01-3554, 1999.
[22] K. Sanada, A. Kitagawa, T. Takenaka, A study on analytical methods by classification of column separations in water pipeline, Trans. Jpn. Soc. Mech. Eng. B 56 (523) (1990) 585–593.
[23] R. Saurel, R. Abgral, A multiphase Godunov method for compressible multifluid and multiphase flows, J. Comput. Phys. 150 (1999) 425–467.
[24] R. Saurel, O. Lemetayer, A multiphase model for compressible flows with interfaces, shocks, detonation waves and cavitation, J. Fluid Mech. 431 (2001) 239–271.
[25] I. Senocak, W. Shyy, A pressure-based method for turbulent cavitating flow computations, J. Comput. Phys. 176 (2002) 363–383.
[26] D.P. Schmidt, C.J. Rutland, M.L. Corradini, A fully compressible, two-dimensional model of small, high speed, cavitating nozzles, Atomization Sprays 9 (1999) 255–276.
[27] H.S. Tang, D. Huang, A second-order accurate capturing scheme for 1D inviscid flows of gas and water with vacuum zones, J. Comput. Phys. 128 (1996) 301–318.
[28] E.F. Toro, Riemann Solvers and Numerical Methods for Fluid Dynamics, Springer Publication Company, 1997.
[29] E.H. Van Brummelen, B. Koren, A pressure-invariant conservative Godunov-type method for barotropic two-fluid flows, J. Comput. Phys. 185 (2003) 289–308.
[30] S. Venkateswaran, J.W. Lindau, R.F. Kunz, C.L. Merkle, Computation of multiphase mixture flows with compressible effects, J. Comput. Phys. 180 (2002) 54–77.
[31] Y. Ventikos, Tzabiras, A numerical method for the simulation of steady and unsteady cavitating flows, Comp. Fluids 29 (2000) 63–88.
[32] G.B. Wallis, One-dimensional Two-phase Flow, McGraw-Hill, New York, 1969.
[33] A.B. Wardlaw, J.A. Luton, Fluid–structure interaction mechanisms for close-in explosions, Shock Vibr. 7 (2000) 265–275.